JIMMA UNIVERSITY

SCHOOL OF GRADUATE STUDIES

COLLEGE OF NATURAL SCIENCES

DEPARTMENT OF CHEMISTRY

SYNTHESIS, CHARACTERIZATION AND PHOTOCATALYTIC APPLICATION OF ZnO-Ag_3PO_4-Fe_2O_3 TERNARY NANOCOMPOSITE

NOVEMBER, 2018

JIMMA, ETHIOPIA

SYNTHESIS, CHARACTERIZATION AND PHOTOCATALYTIC APPLICATION OF ZnO-Ag_3PO_4-Fe_2O_3 TERNARY NANOCOMPOSITE

A FINAL RESEARCH SUBMITTED TO JIMMA UNIVERSITY SCHOOL OF GRADUATE STUDIES IN PARTIAL FULFILLMENT OF THE REQUIREMENTS FOR THE DEGREE MASTERS OF SCIENCE IN INORGANIC CHEMISTRY

BY: AMANUEL G/KIDAN

ADVISOR: GEBRU G/TSADIK (PhD Candidate)

CO-ADVISOR: TILAHUN WUBALEM (M.Sc.)

NOVEMBER, 2018

JIMMA, ETHIOPIA

DECLARATION

I undersigned declare that, this thesis entitled "Synthesis, characterization and photocatalytic application of ZnO-Ag_3PO_4-Fe_2O_3 ternary nanocomposite" is my own original work and it has not been submitted for the award of any academic degree or the like in any other institution or university, and that all the sources I have used or quoted have been indicated and acknowledged.

Name: Amanuel G/Kidan

Signature: _____

Date: _____

The work has been done under the supervision of:

Name: Gebru G/Tsadik (PhD Candidate)

Signature: _____

Date: _____

A FINAL RESEARCH SUBMITTED TO JIMMA UNIVERSITY SCHOOL OF GRADUATE STUDIES IN PARTIAL FULFILLMENT OF THE REQUIREMENTS FOR THE DEGREE MASTERS OF SCIENCE IN INORGANIC CHEMISTRY WAS APPROVED BY

ADVISOR	SIGNATURE	DATE
1. **GEBRU G/TSADIK (PhD Candidate)** College of Natural Sciences Department of Chemistry Jimma University	_____	_____
CO-ADVISOR		
2. TILAHUN WUBALEM (M.Sc.) College of Natural Sciences Department of Chemistry Jimma University	_____	_____
DEPARTMENT HEAD		
3. EPHREM TILAHUN (Asst. Prof.) College of Natural Sciences Department of Chemistry Jimma University	_____	_____

EXAMINERS:

1. External Examiner

_____ _____ _____

2. Internal Examiner

_____ _____ _____

TABLE CONTENTS

Contents **Page**

LIST OF TABLE

Table **Page**

LIST OF FIGURES

Figure **page**

LIST OF APPENDIX TABLES

Table **page**

ABBREVIATION AND ACRONYMS

AOPs	Advanced Oxidation Processes
CB	Conduction Band
Eg	Energy Gap
eV	Electron-Volts
FTIR	Fourier Transforms Infrared Spectroscopy
JCPDS	Joint Committee Powder Diffraction Standard
MB	Methylene Blue
NHE	Normal Hydrogen Electrode
NP	Nanoparticle
UV-Vis	Ultra Violet and Visible Light
VB	Valance Band
XRD	X-Ray Diffraction

ACKNOWLEDGEMENT

I would like to express my deepest and truthful thanks and respect to my advisor Mr. Gebru G/tsadik and my co-advisor Mr. Tilahum wubalem for their significant supervision and expert guidance that greatly inspired me to accomplish this research work.

I would like also to acknowledge and appreciate the chemistry department staff members and Jimma University School of graduate studies, to facilitate conditions for my thesis research work. I wish to gratefully thanks to Dr. Dinsefa Mensur and Mr. Demeke Tesfaye for assisting me in the whole laboratory work to run XRD analysis of the synthesized materials in Adama Science and Technology University, Materials Science and Engineering department. I would like to thank also Mr. Simon Tsegaye for his help in running FTIR spectroscopy, in Ethiopia Pharmaceutical Factory laboratory Addis Ababa.

I also wish to extend my deepest acknowledgement to my family especially my wife Rahwa Gafre, my daughter Saron Amanuel and my brothers Tekle Hadgu, Yemane G/kidan and all my friends for their help in finance and moral support. Finally, I would like to thank Haile Garment Textile Industry to allow me to collect real sample from their waste sewage system and Mr. Tekalgn Bekele and Mr. Abebe Guta in Haile Garment Textile Industry Employers for their special cooperation during entering and getting out to/from the industry.

ABSTRACT

In this work, different types of photocatalysts, single systems; ZnO, Ag_3PO_4, and ternary systems with different molar ratio of ZnO-Ag_3PO_4-Fe_2O_3 were prepared by precipitation method using precursor solutions of Fe_2O_3, ZnO, and Ag_3PO_4. Analysis of crystal structure, energy band gap, functional groups and optical properties of the photocatalysts were characterized by using XRD, FTIR and UV-Visible spectrophotometer instruments respectively. The effects of initial dye concentration, and catalyst load, pH of solution and temperature were investigated. Photocatalytic degradation activities of the synthesized nanocomposites under visible light irradiation have been evaluated in the reduction of aqueous methylene blue (MB) dye solution and real sewage samples collected from Haile Garment Textile Industry. ZnO-Ag_3PO_4-Fe_2O_3 (80:10:10) ternary nanocomposite photocatalyst exhibited the most effective degradation efficiency of methylene blue (MB) dye and real sewage sample at pH= 6, 10 mg/L dye concentration and 140 mg catalyst dose under 50 ^oC 91% and 72% dye was degraded after 150 minute under visible light irradiation.

Keywords: *Methylene blue, Nanocomoposites, Nanoparticle and Photocatalysts*

1. INTRODUCTION

1.1. **Back ground of the study**

Pollutants are foreign substances induced into the environment and bring undesirable effect on environment such as air, water, soil etc. which in turn harm animals and plants as well as human being up to death [1]. Pollutants may be originated from different sources; classified as organic, inorganic or others. Organic pollutants are the major groups of pollutants and becoming an emerging research issue as a result of their hazardous nature and widely spread in wastewater due to varieties of sources like military, domestic wastes as well as industries. Textile industry is the top blamed source of organic pollutants-dyes [2].

Various physical, chemical and biological waste water treatment techniques have been reported [3]. Among these, photo-catalysis is considered as the most relevant cost effective technique that speed up photoreaction with the help of photo-catalyst often semiconductor transition metal oxides such as TiO_2, ZnO, Fe_2O_3, MnO_2, Mo_2O_3 etc irradiating with either UV or Visible light [4]. TiO_2 is the most promising one although its practical application is limited in aqueous media because of its polar surface and weak adsorbing capacity of non-polar organic molecules [5]. ZnO is attracting much attention because of its environmental stability and low cost as well as high photo-catalytic ability but its application is limited only to the UV region; shorter than 378 nm as a result of its wide band-gap in turn limits the use of pure zinc oxide [6]. In addition photocatalytic activity of ZnO is highly affected by photo induced hole-electron pair recombination. Thus, in order to utilize ZnO effectively, its absorption band should be shifted from the UV into the visible region [5].

Photo-catalytic activity of ZnO can be improved by various techniques such as non-metal doping [7], addition of transition metals [8], use of binary and ternary [9] semiconductors. Combining different semiconductor oxides can extend the absorbance range to the visible light region reducing the band gap as well as leads to high photo-catalytic activity [10]. Silver phosphate (Ag_3PO_4), a new type of photocatalyst reported by [11], has been demonstrated to show excellent photocatalytic ability under visible light as well as great photodecomposition of organic compounds. Unfortunately, it is unstable towards photo-illumination as it is easily corroded by photo generated electrons.

($4Ag_3PO_4 + 6H_2O + 12h^+ + 12e^- \rightarrow 12Ag + 4H_3PO_4 + 3O_2$)

Therefore, it is highly desirable to develop effective strategies to improve the stability of the Ag_3PO_4 photo-catalyst. Recent reports indicated that Bi_2MoO_6 [12], SnO_2 [13] and MnO_2 [14] were

successfully used to enhance stability of Ag_3PO_4 based combine nanoparticle. Recently [15] reported that Ag_3PO_4/ZnO binary nanocomposite exhibited more enhanced photocatalytic activity than the single system. Some other literatures also reported about synthesis of binary and ternary mixed oxides [16]. However; to our knowledge, no report has been found on the synthesis and photocalytic application of ZnO-Ag_3PO_4-Fe_2O_3 ternary nanocomposite. Therefore, this study targets to synthesis of ZnO-Ag_3PO_4-Fe_2O_3 ternary nanocomposite and evaluate its photo-catalytic activity on methylene blue dyes under visible light irradiation.

1.2. **Statement of the Problem**

MB dyes discharges into water during its production/application are becoming a major source of environmental contamination due to its toxicity and non biodegradability nature [17]. These dyes have a potential hazard to living organisms. Over exposure to this compound can cause severe injuries to the internal organs of human body including liver, kidneys, lungs and vascular system [18]. As they are resist light, oxidizing agents and heat as well as biodegradation which makes them difficult to remove through conventional water treatment techniques. Researchers have reported photo-catalysis is cost effective alternative for the treatment of waste water containing organic pollutants. ZnO is a good semiconducting material for photo-catalytic application. However, its application is limited to the UV region as result of its wide band-gap. So, the absorption band of ZnO semiconductor can be shift from UV in to visible region by adding narrow band gap transition metal oxides such as Ag_3PO_4 and Fe_2O_3.

Therefore, the study was attempted to answer the following basic research questions:

- To what extent photocatalytic efficiency of ZnO nano particle can be increased by adding Ag_3PO_4 and Fe_2O_3 together?
- What is the effect of dye concentration, pH of the solution, catalyst dose and time on efficiency of ZnO-Ag_3PO_4-Fe_2O_3?
- Is there a significant difference in the photocatalytic performance of ZnO, Ag_3PO_4 and ZnO-Ag_3PO_4-Fe_2O_3 ternary nanocomposite photocatalys?

1.3. Objectives of the Study

1.3.1. General Objective

- To synthesize, characterize and evaluate photo-catalytic activity of ZnO-Ag_3PO_4-Fe_2O_3 of ternary nano-composite.

1.3.2. Specific Objectives

1. To synthesize ZnO-Ag_3PO_4-Fe_2O_3 ternary nanocomposite.
2. To characterize the synthesized nanocomposite using modern spectroscopic techniques such as UV-Vis (single beam) spectrophotometer, FTIR and XRD.
3. To evaluate photo-catalytic activity of ZnO-Ag_3PO_4-Fe_2O_3 ternary nano-composite on degradation of Methylene Blue dyes.
4. To compare photo-catalytic activity of ZnO, Ag_3PO_4 and ZnO-Ag_3PO_4-Fe_2O_3 nanocomposites

1.4. Significance of the study

Now a day, there are a lot of wastes such as organic dyes introduced into the environment raised unwanted effect on human, animals and aquatic life. The findings from this study are expected valuable and cost effective method to synthesis of further new nanophotocatalysts for photocatalytic applications. The main significance of this study could be to prepare cost effective alternative photocatalyst for textile industries to help on removal of toxic and carcinogenic MB dyes from their wastes. The textile industries may treat their wastes using photocatalyst before discharge into water source; it's minimized health risk on human, animals and reduces unwanted change on environment.

There is also an expectation the researchers will use this study as a reference material for further synthesis of new semiconductor nano photocatalyst due to practical interest in air and water remediation, destruction of pathogenic microorganisms, semiconducting, solar cell, gas sensor, ceramic and dental materials under visible light irradiation. Therefore, the finding obtained from this study may also help to giving attention for advancing further research on this particular polymers or inorganic supporters to immobilize the ternary system to enhance the efficiency, attempt potential application in the area of sensors, solar cells, super capacitors, fuel cells etc, and to try other synthesized approaches to fabricate ternary system with nano size and better morphology.

2. LITERATURE REVIEW

2.1. Nanoparticles

Nanoparticles refer to compounds composed of particles with size in 1D ranging from 1 nm to 100 nm [19]. Nanoparticles are used as catalyst and redox active media due to their large surface area to volume ratios and its size/shape depends on optical, electronic and catalytic properties. Moreover, a new kind of nanometer-sized material widely used in the fields of biotechnology, biomedicine and as an efficient adsorbent with large specific surface area and small diffusion resistance. Nano sized semiconductor metal oxides like Al_2O_3, Fe_2O_3, Fe_3O_4, ZnO, MnO_2, Mn_2O_3 and Mn_3O_4 serve as catalysts and/or redox reagents for degradation of organic contaminants. Nano-sized ZnO is direct wide band gap semiconductor with large excitation binding energy about 60ev. Due to variety of attractive physical and chemical properties, it is very important semiconductor for a range of applications such as solar cells [20], gas sensors [21], and catalysts [22].

2.2. **Principles of photo catalytic activity**

Photo-catalysis involves a combination of UV or visible light irradiation and catalysts. Thus, in the photo-catalytic degradation process, organic pollutants are destroyed in the presence of semiconductor photo-catalyst. When a semiconductor absorbs a photon with energy equal or greater than the band gap energy, electrons are transferred from the valence band to the conduction band to produce electron–hole pairs which then encourage the possible reactions with organic pollutants as well as microorganism's cells. The photocatalytic process is quite complicated because the reactions occur in the photocatalysts and on the interface of the photocatalysts and reactants solution [5].

A simple arbitrary description of the photocatalytic process is as followings:

(i). Photon Absorption:

Semiconductors, when absorb photons equal or greater than the material band gap it can generate electrons and holes.

$$\text{Semiconductor} \xrightarrow{hv/heat} e^- \text{ CB} + h^+ \text{ VB} \quad \text{.....1}$$

Semiconductors (e.g., TiO_2, ZnO, Fe_2O_3, WO_3, Ag_3PO_4, CdS, and ZnS) can act as photocatalysts for light-induced redox processes due to their optical properties and electronic structure, which is characterized by an electron filled valence band and an empty conduction band with a appropriate

band gap between them. When a photon with energy of hυ matches or exceeds the band gap energy, Eg, of the semiconductor, an electron, e-, is promated from the valence band to the conduction band, a hole (h^+) is leaved in the valance band [5].

(ii). Recombination

$$e^- CB + h^+ VB \longrightarrow hv/heat \quad \text{.....2}$$

Excited-state conduction-band electrons and valence-band holes can recombine and dissipate the input energy as heat, get trapped in stable surface states, or react with electron donors and electron acceptors adsorbed on the semiconductor surface. In the absence of appropriate electron and hole separation forces, the stored energy is dissipated within a few nanoseconds in the recombination process. When a approprate scavenger or surface defect state is available to trap the electron or hole, recombination is prevented and subsequent redox reactions may occur.

(iii). Formation of free radicals

A. Electrons transfer from the water molecule to the photocatalyst (holes attract electrons in water

Oxidative reaction

$$h^+ VB + OH^- \longrightarrow OH^{\cdot} \quad \text{.....3}$$

This reaction takes place in the valance band of semiconductor. The holes that present in valance band of semiconductor or photocatalyst attract electron from water molecule thus hydroxyl (OH^-) groups are oxidized to $OH^{\cdot}$ (hydroxyl free radical).

B. Electrons transfer from photocatalyst to oxygen dissolved in water:

Reductive reaction

$$e^- CB + O_2 \longrightarrow O_2^- \quad \text{.....4}$$

This reaction takes place in conduction band of semiconductor/ photocatalyst that transfer electrons to oxygen that already dissolved in water, reduction, from O_2 to O_2^- or to -1 oxidation state. It is found that the valence band holes are powerful oxidants (+1.0 to +3.5 V vs NHE (normal hydrogen electrode) depending on the semiconductor and pH), while the conduction-band electrons are good reductants (+ 0.5 to -1.5 V vs NHE). Specially, hydroxyl free radical plays a central role in photocatalysis for wastewater treatment [23]. Due to its high standard potentials of 2.8 V versus NHE in acidic media and 1.55 V versus NHE in basic media, OH radical is highly reactive and non

selective that can oxidize and decompose numerous hazardous compounds to CO_2, water, and inorganic ions [24] and [25].

The most important reactions of semiconductor nanocomposites as a photocatalyst as are follows;

$$\text{Semiconductor} \xrightarrow{hv/heat} e^- \text{ CB} + h^+ \text{ VB} \quad \text{.....1}$$

$$H_2O \longrightarrow H^+ + OH^- \quad \text{.....2}$$

$$h^+ + OH^- \longrightarrow OH^\cdot \quad \text{.....3}$$

$$h^+ + H_2O \longrightarrow OH^\cdot + H^+ \quad \text{.....4}$$

$$e^- + O_2 \longrightarrow O_2^- \quad \text{.....5}$$

$$O_2 + H^+ \longrightarrow HO_2^\cdot \quad \text{.....6}$$

$$2H_2O + O_2^\cdot \longrightarrow 2H_2O_2 \quad \text{.....7}$$

$$H_2O_2 + hv \longrightarrow 2OH^\cdot \quad \text{.....9}$$

$$\text{Organic pollutants} + OH^\cdot \longrightarrow CO_2 + H_2O + \text{Heat} \quad \text{.....10}$$

The produced electron-hole pairs can either recombine and release heat energy or interact separately with other molecules [26]. The electrons in the conduction band can reduce dissolved oxygen to superoxide radical anion (O_2^-) that this radical may form hydrogen peroxide (H_2O_2). The electron reduction of hydrogen peroxide produces hydroxyl radical (OH•) [27]. The holes in the valence band can oxidize the adsorbed water or hydroxide ions to produce hydroxyl radicals (OH•) [28]. Among them the hydroxyl radicals can be used to degrade organic compounds as well as microorganism cells at or near the surfaces of semiconductor catalyst. Adsorbed oxygen at grain surface is an electron capture, which can restrain the combination of electron and hole. The nanoscale catalysts have higher photocatalytic activity than normal material [29].

2.3. **Heterogeneous photo-catalysts**

Heterogeneous catalysis refers to the form of catalysis where the phase of the catalyst differs from that of the reactants. Heterogeneous photo-catalysis includes a large variety of reaction. Photo-catalysis is the acceleration of a photoreaction in the presence of a catalyst. In catalyzed photolysis, light is absorbed by an adsorbed substrate. These reactions occur mostly in heterogeneous

photocatalyst. Most semiconductors are heterogeneous photocatalyts, which have unique characteristics; semiconductors possess a void energy region where no energy levels are available to promote recombination of an electron and hole produced by photo activation in the solid. The energy which extends between the filled valence band and the vacant conduction band is called energy gap [30].

When the semiconductors are absorbed photon with energy equal to or greater than the materials band gap, an electron is excited from the valence band to the conduction band, generating a positive hole in the valence band. The excited electron and hole can recombine and release the energy gained from the excitation of the electron as heat. Recombination is undesirable and leads to an inefficient photocatalyst.

The main goal of the process is to have a reaction between an oxidant with excited electrons to produce a reduced product, and also a reaction between the generated holes with a reductant to produce an oxidized product. Due to the generation of positive holes and electrons, oxidation-reduction reactions take place at the surface of semiconductors. The generated holes are extremely oxidants and should thus be able to oxidize almost all chemicals, as well as water, resulting in the formation of hydroxyl radicals [31].

2.3.1. **Semiconductor photocatalysts**

Semiconductor is characterized by a valance band that filled by electrons and conduction band (empty band) that is separated in energy by an amount Eg, the band from the upper edge of the valance band. Semiconductors are transparent to photon whose energy lies below their band gap and are strongly absorbing for photons whose energy greater than band gap energy. Band to band absorption involves excitation of an electron from valance band to conduction band, resulting in creations of electron hole pair [32]. The surface containing electrons and holes generates Hydroxyl ($OH^{\cdot}$) and other radicals formed by the oxidation of oxygen, water, or hydroxide ions. Thus the direct oxidation of organic pollutants may be possible by photo induced holes. Most of these semiconductor particles have photo-catalytic properties [33] such as the metal oxides, TiO_2, WO_3, ZnO, and Fe_2O_3.

2.4. **Surface modification of ZnO and its as Photo-catalytic application**

ZnO is good semiconductor with wide band gap about (3.3ev) in nature [34]. Nano-sized ZnO has a direct wide-band gap semiconductor with large exaction binding energy of 60ev. Due to variety of

attractive physical and chemical properties, it is a promising candidate photo-catalyst in solar cells gas sensor and catalysts application [35]. ZnO can absorb only UV light with wave length equal or less than 385 nm. So in order to absorb visible light, band gap of ZnO has to be narrowed or split into several sub gaps, which can be achieved by implanting transition metal ions or doping nitrogen [36] and [37].

In recent years many attempts have been made to prepare different ZnO photo-catalyst based nano composites. For example, if two semiconductors are properly integrated into one system, this system can be expected to achieve high photocatalytic activity. So far, a great number of semiconductors with narrow band gaps, such as BiOI, CdS, CuO, V_2O_5, C_3N_4, loaded on the surface of ZnO have been investigated to design visible-light driven composite photocatlysts [38]. The narrow band-gap semiconductors usually act as visible-light sensitizes.

2.5. **Preparation, surface modification and application of Ag_3PO_4**

In recent years, strategies for overcoming the low photocatalytic efficiencies realized with photo catalysts have been developed through design and fabrication of "second generation" photo-catalysts. Ag_3PO_4 has attracted considerable visible light phatocatalyst, and it is a pale yellow semiconductor with a band of 2.45 eV [41]. It has been reported that the CB and VB edge potential of Ag_3PO_4 is 0.45eV and 2.9eV (vs NHE), respectively. The VB potential of Ag_3PO_4 is lower that of ZnO with 2.6 [42], And so Ag_3PO_4 is considered to be an appropriate sensitizer to improve photocatalytic activity in the Ag_3PO_4-ZnO system in which ZnO works as a substrate, while the role of Ag_3PO_4 is sensitizer absorbing visible light. However it has also role in absorbing visible light and improve (enhance) photocataytic activity. Thus large surface area of small sized particles is expected to be beneficial for photocatalytic reactions that mostly occur on the surface of the catalyst [43].

2.6. **Synthesis methods of nano-composites**

There are different methods for synthesis of the nano-sized photo catalyst used for the photo degradation of organic pollutants which may pollute the environment. Some of these are given below.

2.6.1. **Sol gel method**

This process is widely used chemical technique in the fields of materials science and ceramic engineering. Such methods are used primarily for the fabrication of materials (metal oxide) starting from chemical solution that acts as the precursor for an integrated network of either discrete particles

or network polymers or particles may be amorphous or crystalline.

Typical precursors are metal alkoxides which undergo various forms of hydrolysis and poly-condensation reactions. Using inorganic salt or metallic alcohol salt as precursor nano powder can be obtained through gelation process by hydrolytic poly-condensation and some post treatment process. Specifically zinc acetate dihydrate ($Zn(CH_3COO)_2.2H_2O$), 2-methoxyethanol ($CH_2(OCH_3)CH_2OH$) and monoethanolamine ($CH_3CHOHNH_2$) were used as precursor, solvent and stabilizer, respectively. Sol-gel synthesis may be used to prepare materials with a variety of shapes, such as porous structures, thin fibers, dense powders and thin films [44].

2.6.2. **Precipitation method**

Precipitation is one method used in the formation of solid. When the reaction occurs in a liquid solution, the solid formed is called the precipitate. The chemical that causes the solid to form precipitation is called the precipitant. Sometimes the formation of a precipitate indicates the occurrence of a chemical reaction. For example silver nitrate solution is added into a solution of sodium chloride, a chemical reaction occurs a white precipitate of silver chloride is formed. When potassium iodide solution also reacts with lead nitrate solution, a yellow precipitate of lead iodide is formed. Precipitation may occur if the concentration of a compound exceeds its solubility (such as when mixing solvents or changing their temperature). In solids, precipitation occurs if the concentration of one solid is above the solubility limit in the host solid, due to rapid quenching or ion implantation, and the temperature is high enough that diffusion can lead to segregation into precipitates. Precipitation in solids mostly used to synthesize nano clusters [45]. Precipitation reaction applied for different application, such as for making pigments, removing salts from water in water treatment, and in classical qualitative inorganic analysis. Precipitation is also useful to isolate the products of a reaction during work up. Ideally, the product of the reaction is insoluble in the reaction solvent. Thus, it precipitates as it is formed, preferably forming pure crystals [5].

2.6.3. **Hydrothermal method**

Hydrothermal synthesis includes the various techniques of crystallizing substances from high temperature aqueous solutions at high vapor pressures. Hydrothermal synthesis can be defined as a method of synthesis of single crystals that depends on the solubility of minerals in hot water under high pressure. The crystal growth is performed in an apparatus consisting of a steel pressure vessel called an autoclave in which a nutrient is supplied along with water. A temperature gradient is maintained between the opposite ends of the growth chamber. At the hotter end the nutrient solute

dissolves, while at the cooler end it is deposited on a seed crystal, growing the desired crystal. Thus zinc acetate dehydrate ($Zn(C_2H_3O_2)_2 \cdot 2H_2O$), citric acid and ethanol (CH_3CH_2OH) aqueous solutions were used a precursor, stabilizer and solvent, respectively for the synthesis of the photocatalyst.[46]

2.6.4. **Impregnation method**

Catalyst support is the material, usually a solid with a high surface area, to which a catalyst is affixed. The activity of heterogeneous catalysts and nano material based catalysts occurs at the surface atoms. Consequently, great effort is made to maximize the surface area of a catalyst by distributing it over the support. The support may be inert or participate in the catalytic reactions. Typical supports include various kinds of carbon, alumina, silica and organic polymer [47]. In impregnation techniques, the support is contacted with a precursor solution, in other word impregnation is related to ion exchange (adsorption processes) and the interaction with the support is dominant. Thus, low loadings, often for precious metals, are achieved by adsorption of the precursor molecules onto surface groups of the support (ion adsorption) or through the exchange of ions in, for example, zeolites (ion exchange), after which excess precursor is removed. When higher loadings are required, the washing step is skipped and the support is directly dried, so that all precursor ends up on the support (impregnation and drying). Impregnation can be performed to incipient wetness, whereby the pores of the support are filled with precursor solution, to prevent deposition on the external surface of the catalyst grains and to limit waste [48].

2.7. **Characterization of photocatalyst**

Crystal structure is one of the most important aspects of materials science and engineering as many properties of materials depend on their crystal structures. The basic principles of many materials characterization techniques such as XRD, Transmission electron microscopy (TEM) are based on crystallography [49]. Therefore, understanding the basics of crystal structures is key concept.

2.7.1. **X-Ray diffraction**

X-ray diffraction is a non-destructive analytical technique that can be applied for the identification of unknown specimens and for the determination of materials properties. It is the most important and beneficial technique in solid state chemistry and it has been applied for the finger print characterization of crystals and for the determination of their structures.

X-ray diffraction has been one of the basic and most useful tools for characterization. Initially X-ray diffraction was used to answer simple questions such as: “have I made a new material?”Or: “has the

crystallization process gone to completion?" Early attempts at determining crystal structures using X-ray diffraction were often unsuccessful because many of these early synthetic materials were available only as powder samples. This method requires an X-ray source (mono-chromatic or of variable), the sample (single crystal, powder or solid piece) which is under investigation and a detector (radiation counter or photographic film) that takes the diffracted X-rays. [50].

2.7.2. **Fourier transforms Infrared**

Fourier transforms Infrared (FTIR) spectroscopy is a measurement technique that allows one to record infrared spectra. A basic IR spectrum is essentially a graph of infrared light absorbance (or transmittance) on the vertical axis vs. frequency or wavelength on the horizontal axis. Typical units of frequency used in IR spectra are reciprocal centimeters (sometimes called wave numbers). Thus, the mid infrared, approximately 4000-400 cm^{-1} may be used to study the fundamental vibrations and associated rotational vibrational structure. Thus, IR spectroscopy often used to identify structures because functional groups give rise to characteristic bands both in terms of intensity and position (frequency). In infrared spectroscopy, IR radiation is passed through a sample. Some of the infrared radiation is absorbed by the sample and some of it is passed through (transmitted). The resulting spectrum represents the molecular absorption and transmission, creating a molecular fingerprint of the sample. Like a fingerprint no two unique molecular structures produce the same infrared spectrum. Furthermore, an infrared spectrum represents a fingerprint of a sample with absorption peaks which correspond to the frequencies of vibrations between the bonds of the atoms making up the material. Because each different material is a unique combination of atoms, no two compounds produce the exact same infrared spectrum. Therefore, infrared spectroscopy can result in a positive identification (qualitative analysis) of every different kind of material. In addition, the size of the peaks in the spectrum is a direct indication of the amount of material present.

2.8. **Effect of Operational Parameters**

There are different factors which may affect photocatalytic efficiency of a photocatalysts under UV as well as solar radiations. Because, photocatalytic reactions are extremely complex processes involving many participants namely water, organic substrate, catalyst, light and oxygen. These factors are: Influence of various parameters including, pH of solution, Catalyst Loading, Initial Concentration and Nature of Pollutants.

2.8.1. **Effect of pH**

A solution pH is one of the most important operating parameters that affect the charge, size of aggregates and the position of conductance and valance bands [51]. Many reports have used the point of zero charge (PZC) of TiO_2 to study the pH impact on the photocatalytic oxidation performance. Thus, the point of zero discharge (PZC) for the most commonly used form of TiO_2 is 6.9 [52]. When operating pH < PZC (TiO_2), the surface charge for the catalyst becomes positively charged and gradually exerted an electrostatic attraction force towards the negatively charged compounds (pollutants). At pH >PZC (TiO_2), the catalyst surface becomes negatively charged and repulse the anionic compounds in water or gradually exerted an electrostatic attraction force towards the positively charged compounds in water (pollutants).

At pH < PZC: $TiOH + H^+ \longrightarrow TiOH_2^+$.....1

At pH > PZC: $TiOH + OH^- \longrightarrow TiO^- + H_2O$.....2

Therefore the surface of the TiO_2 is positively charged under acidic conditions and negatively charged under alkaline conditions. The maximum oxidizing capacity of the titania is at lower pH however the reaction rate is known to decrease at low pH due to excess H^+ [53]. The selection of pH is thus needed to be appropriate in order to achieve maximum degradation efficiency.

2.8.2. **Catalyst Loading Effect**

A catalyst dose linearly dependency holds until certain extent when the reaction rate starts to aggravate and becomes independent of TiO_2 concentration. The excess TiO_2 particles can create a light screening effect that reduces the surface area of TiO_2 being exposed to light illumination and the photo-catalytic efficiency. Therefore, any chosen photo-reactor should be operated below the saturation level of TiO_2 photo-catalyst used to avoid excess catalyst and ensure efficient photons absorption. For example, the effect under the amount of ZnO nano powder was reported that was on the photo-degradation efficiency of methyl orange from aqueous solution by UV irradiation and found that the photo degradation efficiency increases with an increase in ZnO nano powder concentration up to 160 mg/L, and then decreased. This observation was explained in terms of availability of active sites on the catalyst surface and the penetration of UV light into the suspension. Generally, in any given photocatalytic application, the optimum catalyst concentration must be determined, in order to avoid excess catalyst and ensure total absorption of efficient photons [54].

This is because an unfavorable light scattering and reduction of light penetration into the solution is observed with excess photocatalyst loading.

2.8.3. **Initial Concentration and Nature of Pollutants**

The rate of photocatalytic degradation of certain pollutant depends on its nature and concentration. A number of studies have reported the dependency of the TiO_2 reaction rate on the concentration of contaminants in water [55]. High concentration of pollutants in water saturates the TiO_2 surface and hence reduces the photonic efficiency and that result deactivation of the photocatalyst. In addition to the concentration of pollutants, the chemical structure of the target compound also influences the degradation performance of the photocatalytic reactor. For example, 4 chlorophenol requires prolonged irradiation time due to its transformation to intermediates compared with oxalic acid that transforms directly to carbon dioxide and water. Therefore, the photocatalytic degradation of aromatics is highly dependent on the substituent group [56]. The organic substrates with electron withdrawing nature (benzoic acid, nitrobenzene) strongly adhere to the photocatalyst and these are more susceptible to direct oxidation compared with the electron donating groups [57].

2.9. **Methylene blue (MB) dyes as pollutants**

Methylene blue is a heterocyclic aromatic chemical compound with molecular formula: $C_{16}H_{18}ClN_3S$. It has many uses in a range of different fields. At room temperature it appears as a solid and is odorless and a dark green powder, when dissolved in water which yields a blue solution. When dissolved in water, the UV-visible spectrum of MB showed three absorption maxima. The first band was observed at 246 nm and then 291 nm and more intensely 665 nm. The absorption maxima wavelength of MB (λ_{max} = 291 and 665 nm) was used for the analysis during degradation and decolorization of MB dye, respectively. The natural pH of the aqueous dye solution is 6.5. The pH of the solutions can be adjust using H_2SO_4 or NaOH.

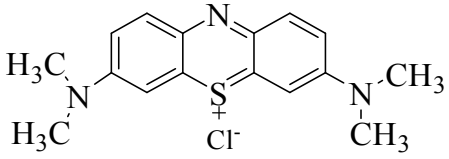

Figure 1. Structural formula of Methylene blue.

The radicals can attack the C–S^+=C functional group in MB, which is in direct Coulombic interaction with the surface of photo catalyst. Therefore, the initial step of MB degradation can be ascribed to the

cleavage of the bonds of the C–S^+=C functional group in MB. The passage from C–S^+=C to C–S (=O)–C requires the conservation of the double bond conjugation, which induces the opening of the central aromatic ring containing both hetero atoms, S and N. The origin of H atoms necessary to C–H and N–H bond formation can be proposed from the proton reduction by photo-generated [58]. The hydroxyl radical existing on the surface of photocatalyst accelerated the degradation of MB.

$R–S^+=R + OH\circ \rightarrow R–S(=O)–R + H^+$ ……. 10

The sulfoxide group can undergo a second attack by an OH◦ radical producing the sulfone (non-detected) and causing the definitive dissociation of the two benzenic rings.

$NH_2–C_6H_3(R)–S(=O)–C_6H_4–R + OH\circ \rightarrow NH_2–C_6H_3(R)–SO_2 + C_6H_5–R$ …… 11

And/or

$NH_2–C_6H_3(R)–S(=O)–C_6H_4–R + OH\circ \rightarrow NH_2–C_6H_4–R + SO_2–C_6H_4–R$…… ……12

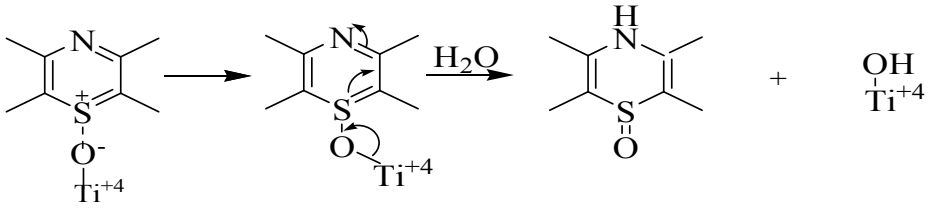

Figure 2. Electronic reorganization during the passage of MB adsorbed to the sulfoxide form.

The oxidation degree of sulfur has now increased from 0 to +5. Subsequently, the sulfone can be attacked itself by a third OH◦ radical for giving a sulfonic acid.

$SO_2–C_6H_4–R + OH\circ \rightarrow R–C_6H_4–SO_3H$ ……..13

Presently, sulfur has reached its final, stable and maximum oxidation degree (+6) and the final release of $SO4^{2-}$ ions can be attributed to a fourth attack by OH◦

$R–C_6H_4–SO_3H + OH\circ \rightarrow R–C_6H_4\circ + SO4^{2-} + 2H^+$ ……..……...14

Radical $R–C_6H_4\circ$ can subsequently react either with OH◦ giving a phenolic compound (figure 2) or with a H◦ radical generated by reaction (11).Concerning the mineralization of the three nitrogen-containing groups in MB molecule; two cases have to be examined. First, the central imino-group undergoes a N=C double bond cleavage induced by the cleavage of the double bond of the $–S^+=$ group in para position in the central aromatic ring.

3. METHODOLOGY

3.1. Experimental Sites

Synthesis of ZnO, Ag_3PO_4 and ZnO-Ag_3PO_4-Fe_2O_3 nano materials and the studies of photocatalytic activity as well as UV-Vis spectrophotometer characterization were conducted at Jimma University Chemistry Research Laboratory and programmable furnace was used in Jimma University, college of Agriculture and Veterinary Medicine, Animal Nutrition laboratory. FTIR were conducted at Ethiopia Pharmaceutical Factory laboratory Addis Ababa. XRD was conducted at Adama Science and Technology University, Materials Science and Engineering department laboratory.

3.2. Chemicals and Reagents

All chemicals were analytical grade reagents and used without further purification. Zinc nitrate hexahydrate (Zn $(NO_3)_2.6H_2O$), Na_2CO_3, Iron nitrate nanohydrate (Fe $(NO_3)_3.9H_2O$), $AgNO_3$ and $Na_2HPO_4.2H_2O$ were used to prepare the precursors solutions of Fe_2O_3, ZnO and Ag_3PO_4, respectively. Ethanol also was employed to wash the precipitate and distilled H_2O to prepare solutions. NaOH, HCl and buffer solution used to adjust pH of the solution. Methylene Blue dye was used as a reference (model) of organic contaminant for investigating photo catalytic activities of the synthesized photo catalysts.

3.3. Apparatuses and Instruments

The structures of the synthesized nano material were examined by powder X-ray diffraction (SHIMADZU,700, from Japan) using with an X-ray source of a Cu Kα radiation (wavelength of 0.15406 nm) at step scan rate of 0.02 (step time: 1 s; 2θ range: 10-80^o.). Sizes of the particles were calculated by the Scherer's equation using the most intense peak of as the synthesized nanocomposites. The determination of functional groups of the as synthesized nanocomposites was made using FTIR spectroscopy. The band gaps of the all as synthesized nanocomposites were determined using UV-Visible spectrophotometer (JENWAY, 6705, from UK). Programmable furnace (Mattif, Shimazu, Japan), Ceramic crucibles, volumetric flasks, Pipettes, Magnetic stirrer, Measuring cylinder, Beakers and other glass wears were also used for the determination of photocatalytic degradation efficiency of the prepared samples.

3.4. **Preparation of Zinc Oxide Nanoparticles.**

Into two separate beakers, zinc nitrate hexahydrate (0.1 mol, 29.74g) and 0.1mol, (10.6g) Na_2CO_3 were dissolved in 100 mL of distill water. Then, Zn $(NO_3)_2.6H_2O$ solution was slowly added into Na_2CO_3 solution and the mixture was stirred continuously for 2 h. The resulting precipitate was allowed to settle down for 24 h, filtered by Whatman 540 filter paper and washed by distilled water and ethanol. Then, the precipitate was dried at 100 ^oC for 12 h and calcinated at 350 ^oC for 12 h in programmable furnace to get the white powder ZnO nano particles [59].

3.5. **Preparation of Ag_3PO_4 Nanoparticles**

Ag_3PO_4 was prepared by chemical precipitation method in the dark using silver nitrate ($AgNO_3$) and disodium hydrogen phosphate ($Na_2HPO_4.2H_2O$) as raw materials. The $AgNO_3$ solution (solution [A]) was prepared by dissolving 0.1mol (17.1 g) of $AgNO_3$ powder in 100 mL distill water in dark condition. Similarly Na_2HPO_4 solution (solution [B]) was prepared by dissolving 0.1mol (17.8 g) of Na_2HPO_4 powder in 100 mL distill water. Then after, solution [A] was added drop by drop into solution [B] with continuous stirring for 3 hour in dark room and the precipitation so generated was made to settle down for 12 h. The resulting precipitate was filtered from the mother liquor and washed with distilled water followed by ethanol. It was then, dried at 60 ^oC for 12 h and finally calcined at 300 ^oC for another 2 h and kept in a container as Ag_3PO_4 [5].

3.6. **Synthesis of ZnO-Ag_3PO_4-Fe_2O_3 Nanocomposites**

The nanocomposite ZnO-Ag_3PO_4-Fe_2O_3 photocatlyst were synthesized with different molar composition by mixing the following solutions: 0.1M $Zn(NO_3)_2.6H_2O$, 0.1M Na_2CO_3, 0.1M $Na_2HPO_4.2H_2O$ with 0.1M $AgNO_3$ and 0.1M $Fe(NO_3)_3.9H_2O$. First, the ternary system ZnO-Ag_3PO_4-Fe_2O_3 (80:10:10) were prepared by dissolving 0.1M (1.71g) $AgNO_3$ and 1.78 g (0.1M) Na_2HPO_4 dissolved in 100 mL of distill water into two separate beakers. Secondly, 1.06 g Fe $(NO_3)_3.9H_2O$ was dissolved in 100 mL of distill water separately. These two precursor solutions of Ag_3PO_4 and Fe_2O_3 were mixed using magnetic stirrer with continuous stirring for 2 h.

Thirdly, in to two separate beakers, 23.8 g (0.1M) Zn $(NO_3)_2.6H_2O$ and 8.348 g (0.1M) Na_2CO_3 were dissolved in 100 mL of distill water. Similarly, these two solutions were mixed with continuous stirring for 2 h. Then, the ZnO precursor solution was mixed with above solution comprising the precursors of Ag_3PO_4 and Fe_2O_3. The mixture solutions were continuously stirred for 30 minute at

room temperature until the formation of homogenous solution. The prepared mixture was left to stand for 24 h for the formation of settled precipitate of the mixture. The resulting precipitate was washed with distill water, with ethanol and then allowed to dry at 100 ^{o}C for 12 h. Finally, the dried sample was calcinated at 350 ^{o}C for 3 h. Similar procedure was applied for the preparation of other samples ZnO-Ag_3PO_4-Fe_2O_3 (85:15:5), ZnO-Ag_3PO_4-Fe_2O_3 (70:20:10), by adjusting the molar ratio as described above.

3.7. **Characterization of photo-catalysts**

The as-synthesized photo-catalysts were characterized for absorption (band gap), structure and crystallinity, and functional group by UV-Vis, XRD, and FTIR.

3.7.1. **UV-Visible spectrophotometer analysis**

The optical absorption spectra and band gap of the synthesized photo-catalysts was determined using UV-Vis spectrophotometer at Jimma University chemistry research laboratory. Then the absorbance of the photo-catalyst solution was measured using a quartz tube, scanning over 200-800 nm.

3.8. **Photo-catalytic degradation studies of Methylene Blue**

Photocatalytic degradation of methylene blue (MB) was carried out at optimum temperature. Appropriate amount of the as-synthesized photo catalyst powder and aqueous solution of MB were taken in a reactor tube. The suspension was also constantly stirred for 30 min in the dark before irradiation to reach at absorption equilibrium. During the irradiation, the photo reactor was maintained under magnetic stirring for achieving a homogeneous suspension to promote the adsorption of dye on the surface of photocatalysts [60]. A fluorescent lamp that predominantly emit with the definite power 65 W, 220 Volts and 50 Hz frequency was employed as source of visible radiation and positioned parallel to the reactor. 10 ml of each sample was drawn at 30 minutes interval. Here also the suspension was centrifuged at 3000 rpm for 20 minutes and filtered to remove the catalyst particles before measuring absorbance using quartzes cells. Decolorization was observed in terms of change in intensity of the dyes at λ_{max} (665nm). The percent degradation of dyes was calculated by the following equation [62]:

$$\% \text{ degradation} = \frac{A_o - A_t}{A_o} \text{ X } 100$$

Where A_o is absorbance of dye at initial stage, A_t is absorbance of dye at time “t”.

4. RESULTS AND DISCUSSION

4.1. Characterization of the synthesized photocatalyst

4.1.1. Analysis of the XRD Patterns

XRD Patterns of the synthesized samples of ZnO, Ag_3PO_4, ZnO-Ag_3PO_4-Fe_2O_3 (80:10:10), ZnO-Ag_3PO_4-Fe_2O_3 (70:20:10), ZnO-Ag_3PO_4-Fe_2O_3 (80:15:5) are shown in Figures 5a-f. Accordingly, diffraction peaks observed at scattering angle 2θ=31.8411^o (1 0 0), 34.4724^o (0 0 2), 36.3142^o (1 0 1), 47.606^o (1 0 2), 56.6570^o (1 1 0), 62.8965^o (1 0 3), 66.4439(2 0 0), 68.0094^o (0 1 2), 69.1180^o (2 0 1) and 76.9918^o (2 1 1) represent hexagonal wurtzite structure of ZnO. All characteristic peaks observed for ZnO NPs are in good agreement with those taken from the joint committee of powder diffraction standards (JCPDS) card No.36-1451. Diffraction peaks related to impurity are not observed in the XRD patterns, confirming the purity of the synthesized product.

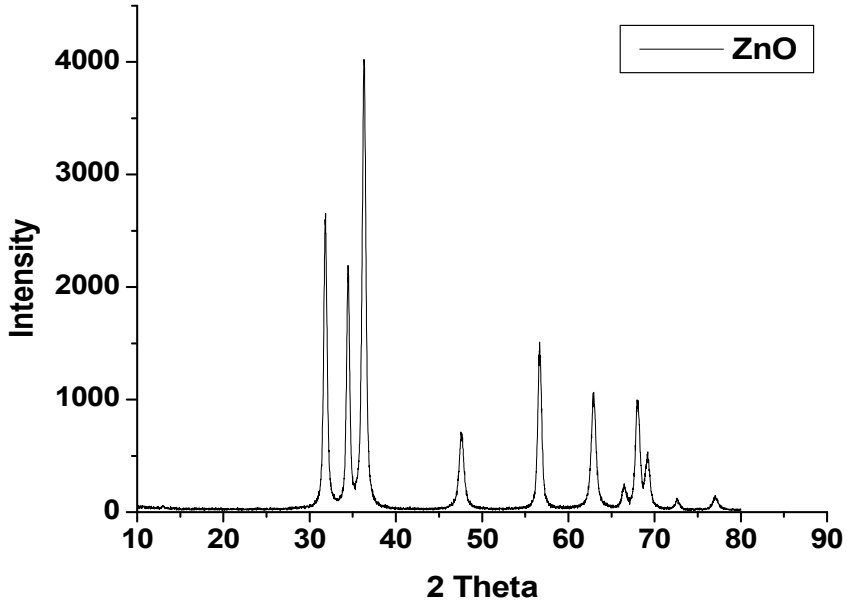

Figure 3a. XRD patterns of ZnO nanoparticle

The diffraction peaks observed at 21.0758^o (1 1 0), 29.8828^o (2 0 0), 33.4802^o (2 1 0), 36.762^o (2 1 1), 47.9751^o (3 1 0), 52.8643^o (2 2 2), 55.1914o (3 2 0), 57.4525^o (3 2 1), 61.8211^o (4 0 0), 70.0680^o (4 2 0) and 72.0583^o (4 2 1) indexed to the body centered cubic structure of Ag_3PO_4. All characteristic peaks observed for Ag_3PO_4 NPs are in good agreement with those taken from the joint committee of powder diffraction standards (JCPDS) card No. 87-1164. Diffraction peaks related to impurity are not observed in the XRD patterns, confirming the high purity of the synthesized product.

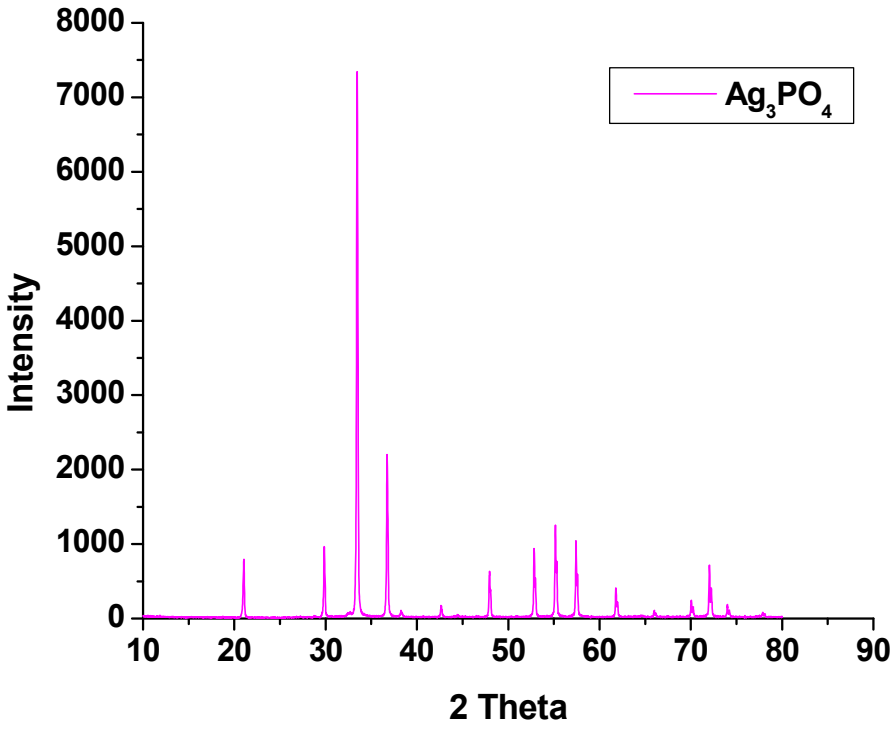

Figure 3b. XRD patterns of Ag_3PO_4 Nanoparticle

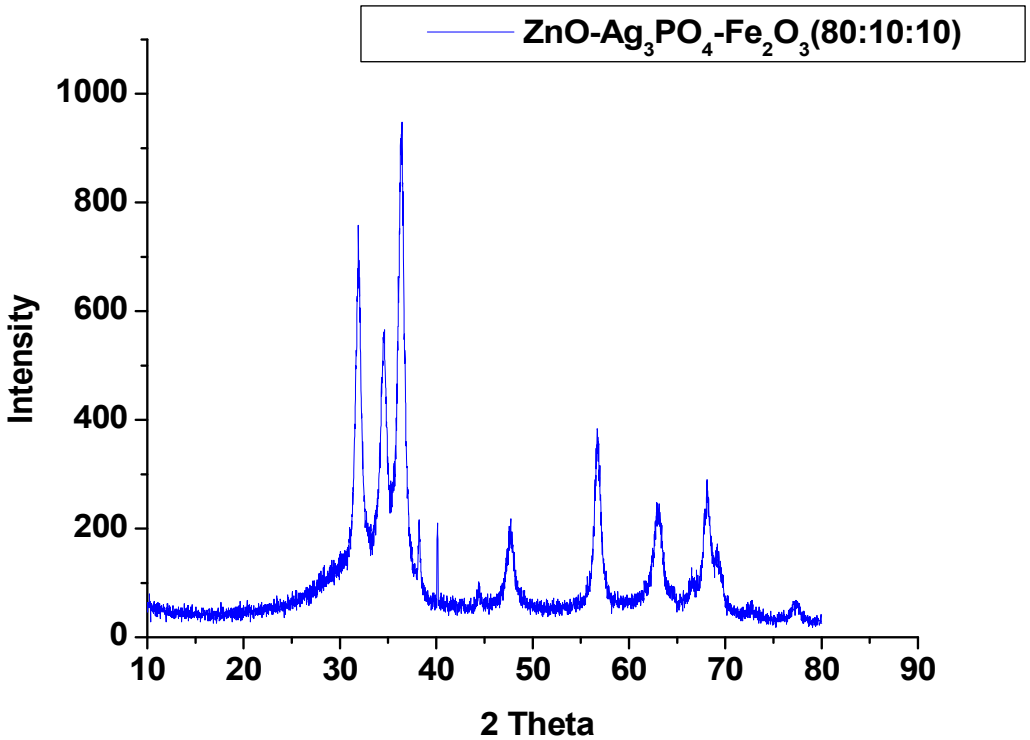

Figure 3c. XRD patterns of ZnO-Ag_3PO_4-Fe_2O_3 (80:10:10)

The ternary systems ZnO-Ag_3PO_4-Fe_2O_3 (80:10:10) diffraction peaks were observed at 2θ values of 30.3429°, 31.9282°, 34.5581°, 36.3638°, 38.2022°, 40.3811°, 46.7898°, 47.6643°, 55.6459°, 56.7217°, 57.1751°, 62.9817°, 66.5223°, 68.0675°, 69.0015° and 77.2443°. Among these, diffraction peaks at 31.9282°, 34.5581°, 36.3638°, 47.6643°, 56.7217°, 62.9817°, 66.5223°, 68.0675°, 69.0015° and 77.2443° could be attributed to hexagonal wurtzite structure of the crystal of ZnO and peaks at 2θ values of 30.3429°, 46.7898°, 55.6459°, and 57.1751° could be ascribed to body centered cubic structure of Ag_3PO4 and the peak at 2θ values 40.3811° was observed due to hexagonal crystal structure Fe_2O_3 (JCPDS card no. 87-1164) The other peaks observed at 2θ values are 38.2022° may be resulted from impurity (Aluminum foil) during sample preparation.

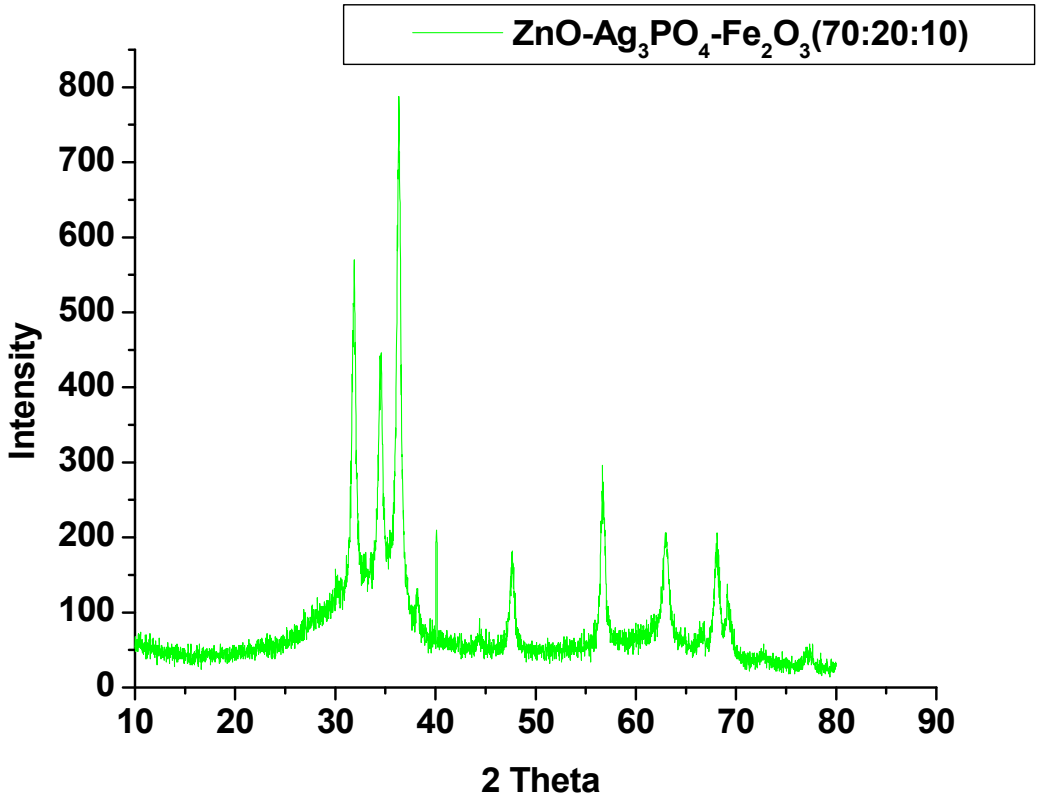

Figure 3d. XRD patterns of ZnO-Ag_3PO_4-Fe_2O_3 (70:20:10)

In the case ZnO-Ag_3PO_4-Fe_2O_3 (70:20:10) diffraction peaks appeared at 2θ= 30.1232°, 31.0820°, 31.8725°, 32.9999°, 33.4993°, 34.5283°, 36.3371°, 37, 2360°, 38.2052°, 40.3861°, 47.6519°, 56.6941°, 57.3453°, 61.6638°, 62.9709°, 63.5832°, 66.3423°, 66.7022°, 67.5820°, 68.0708°, 69.1848° and 76.9993°. Among these, diffraction peaks at 31.8725°, 34.5283°, 36.3371°, 56.6941°, 62.9709°, 66.7022°, 68.0708°, 69.1848° and 76.9993° responsible to wurtzite structure of ZnO. The other peaks observed at 2θ values are 38.2022° may be resulted from impurity (Aluminum foil) during sample preparation.

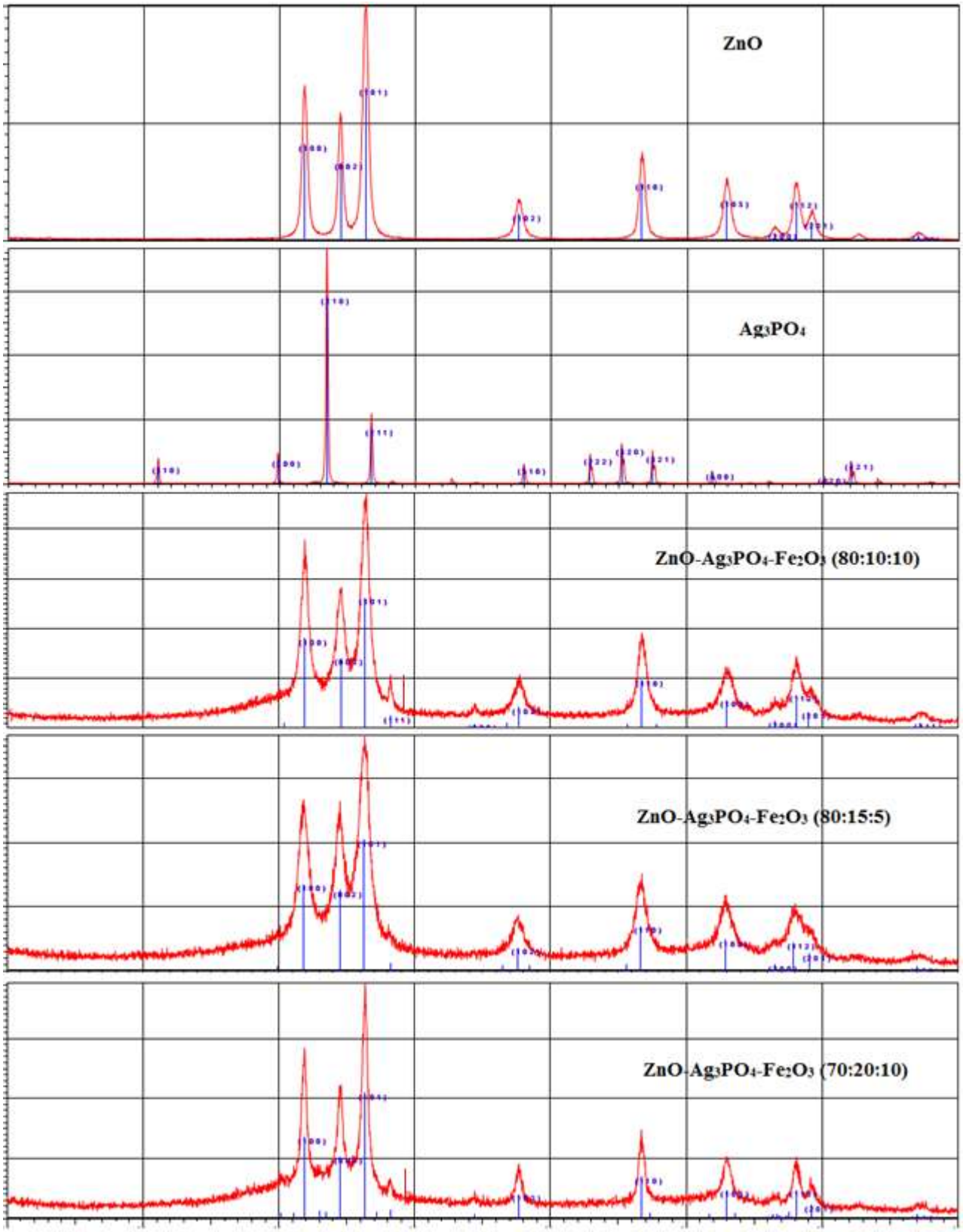

Figure 3e. Summery XRD patterns of ZnO, Ag_3PO_4 and ZnO-Ag_3PO_4-Fe_2O_3 with different molar ratio

The ternary systems ZnO-Ag_3PO_4-Fe_2O_3 (80:15:5) diffraction peaks were observed at 2θ values of 29.8835°, 31.8835°, 34.5031°, 36.2702°, 38.2352°, 46.4699°, 47.5859°, 48.4889°, 55.5859°, 56.6230°, 62.8834°, 66.5223°, 67.0675°, 69.9019° and 76.9793°. Among these, diffraction peaks at 31.8835°, 34.5031°, 36.2702°, 47.5859°, 56.6230°, 62.8834°, 66.5223°, 69.9019° and 76.9793° responsible to wurtzite structure of ZnO and the peaks 29.8835°, 55.5859°, described to body centered cubic structure of Ag_3PO4. No peak is observed attributable to Fe_2O_3 possibly due to small concentration (5%) of the former and amorphous nature of the later. The other peaks observed at 2θ values are 38.2022° may be resulted from impurity (Aluminum foil) during sample preparation.

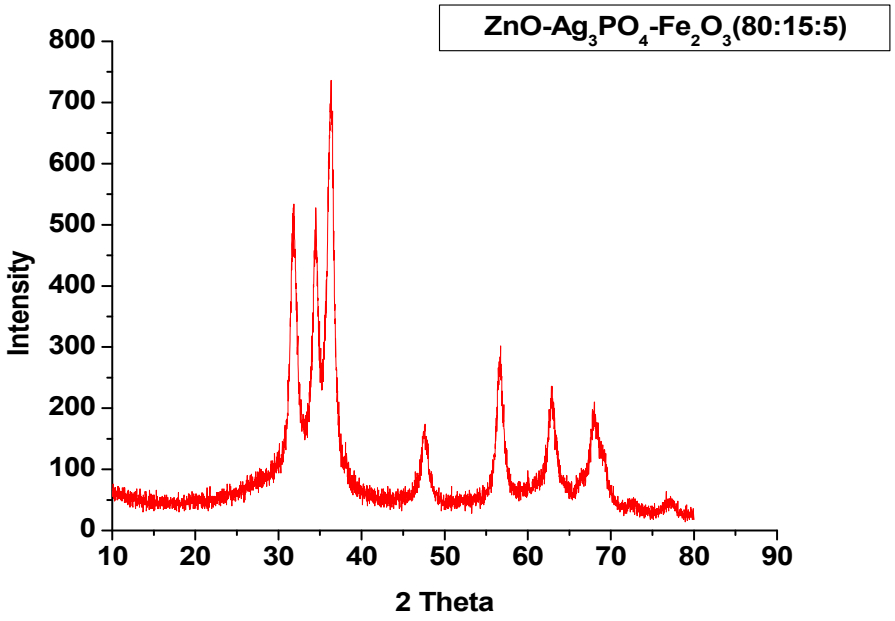

Figure 3f. XRD patterns of ZnO-Ag_3PO_4-Fe_2O_3 (80:15:5)

Average crystallite size of each of the as-synthesized ZnO, Ag_3PO_4, ZnO-Ag_3PO_4-Fe_2O_3 (80:15:5), ZnO-Ag_3PO_4-Fe_2O_3 (80:10:10), ZnO-Ag_3PO_4-Fe_2O_3 (70:20:10) nanocomposites was calculated using the Debye-Scherrer's formula;

$$D = \frac{K\lambda}{\beta \cos\theta} \quad \text{.....4.1}$$

Where, **D**= crystallite size in nm, **K**= the shape factor constant taken as 0.9; **β** is the full width at half maximum (FWHM) in radians, **λ** is the wave length of the X-ray (0.15406 nm) for Cu target Kα1 radiation and **θ** is the Bragg's angle. The calculated average crystalline size of as-synthesized photocatalysts confirm the involvement the good crystalline range between 10 and 50 nm [63] as summarized in Table 1 below.

Table 1. Calculated crystal sizes of the synthesized Photocatalysts

Photocatalyst	2θ(degree)	cos θ	β(radians)	D(nm)	Band gap(eV)
ZnO	36.3142	0.9502	0.0089	16.3	3.29
Ag3PO4	33.4802	0.9576	0.0023	62.9	2.42
ZnO-Ag_3PO_4-Fe_2O_3 (80:10:10)	36.3638	0.9500	0.0139	10.5	2.34
ZnO-Ag_3PO_4-Fe_2O_3 (80:15:5)	36.2702	0.9503	0.0076	19.1	2.36
ZnO-Ag_3PO_4-Fe_2O_3 (70:20:10)	36.3371	0.9501	0.0087	16.9	2.35

4.1.2. **UV-Visible Spectra of the Synthesized Photocatalysts**

The band gap energy (Eg) of nanoparticle and nanocomposites can be calculated by using the well known formula given below [71].

$$E_g = \frac{hc}{\lambda max} \quad \text{.....4.2}$$

Where Eg is the band gap energy required to excite the electron from VB to CB in electron volt and λmax is wavelength in nanometer for the maximum absorption edge. The λ_{max} of ZnO, Ag_3PO_4 and ZnO-Ag_3PO_4-Fe_2O_3 (80:10:10) ZnO-Ag_3PO_4-Fe_2O_3 (80:15:5) and ZnO-Ag_3PO_4-Fe_2O_3 (70:20:10) were appeared at 377 nm, 512, 530, 524 and 528 using by ratio solvent Ethanol and distill water.

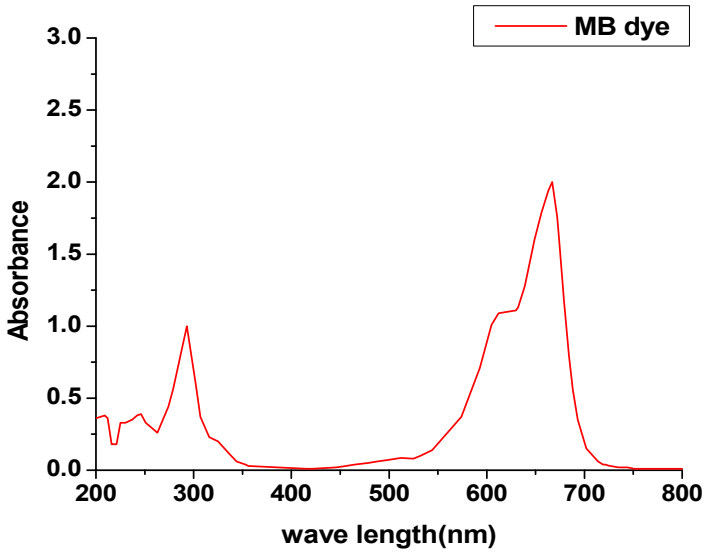

Figure 4a. UV-Visible absorption maxima of aqueous MB solution

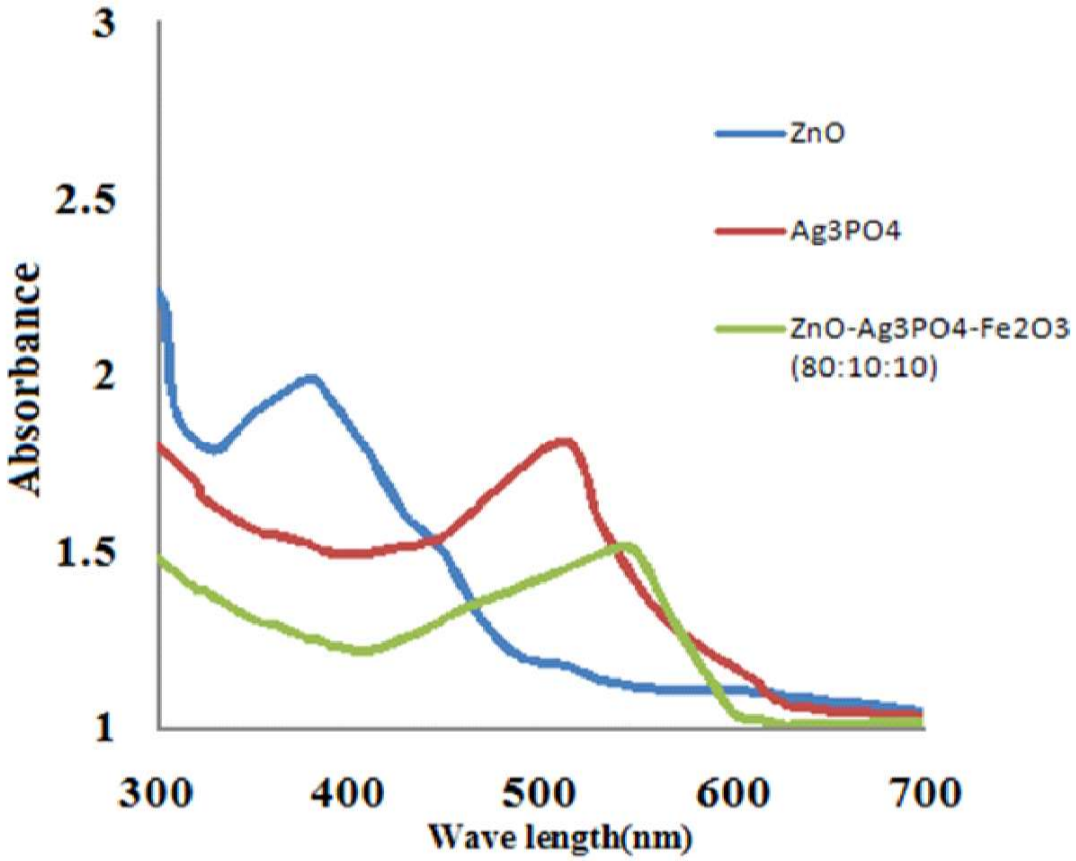

Figure 4b. UV-Visible absorption spectra of ZnO, Ag3PO4, and ZnO-Ag_3PO_4-Fe_2O_3 (80:10:10)

Based on [71] equation the band gaps of the synthesized materials such as ZnO and Ag_3PO_4 are found to be 3.29 eV and 2.42 eV.

$$E_g = \frac{4.135667 \times 10^{-15}(eV.s) \times 3 \times 10^{8}(ms^{-1})}{337 \times 10^{-9}(m)} = 3.29\ eV$$

The results obtained as such are in good agreement with the previously reported works [65].The band gap of selected ZnO-Ag_3PO_4-Fe_2O_3 (80:10:10**)** ternary nanocomposite is equals to 2.34 eV. As can be noted here, formation of ternary systems resulted in further red-shift in the visible spectrum. Based on the band gap results of the ternary systems, ZnO-Ag_3PO_4-Fe_2O_3 (80:10:10) was selected for photocatalytic application. In this case, the absorption band gap of ternary ZnO-Ag_3PO_4-Fe_2O_3 (80:10:10) nanocomposite further to the visible region making it a better visible active nanocomposite photocatlyst.

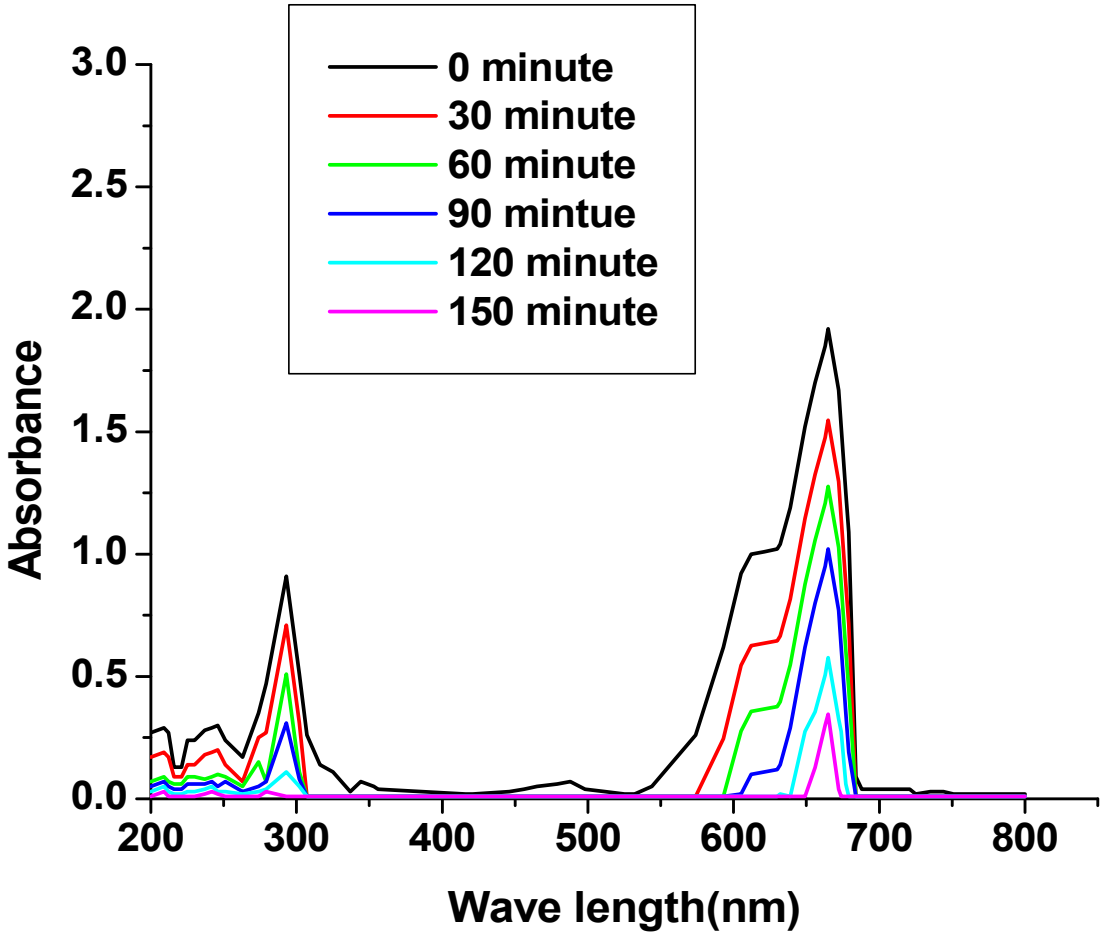

Figure 4c. UV-Vis absorption spectra of 20 mg/L MB dyes at different irradiation time

4.1.3. Analysis of the IR Spectra of the Synthesized Photocatalysts

The FTIR spectral patterns of the ZnO and ZnO-Ag_3PO_4-Fe_2O_3 (80:10:10) nanocomposites are depicted in Figure 5 a &b. Peaks observed at 2855 cm^{-1} and 2925 cm^{-1} can be ascribed to symmetric and asymmetric C-H stretching vibrations respectively, the appearance of which could be attributed to the presence of residual hexanes which used to wash sample holder during FTIR characterization. The peaks observed at 1461 and 1377 cm^{-1} could be ascribed to the bending vibration of C-H groups which resulted from a residual hexane that used to wash the nanocomposite and it was confirmed similar report made by [64]. The strong absorption bands between 956 cm^{-1} observed in cases attributed to P-O stretching vibrations of phosphate groups (PO_4^{3-}) resulted from Ag_3PO_4, one of the component in the ternary nanocomposite system [65].The absorption band observed at 551 cm^{-1} in indicate stretching mode of metal oxide [66].

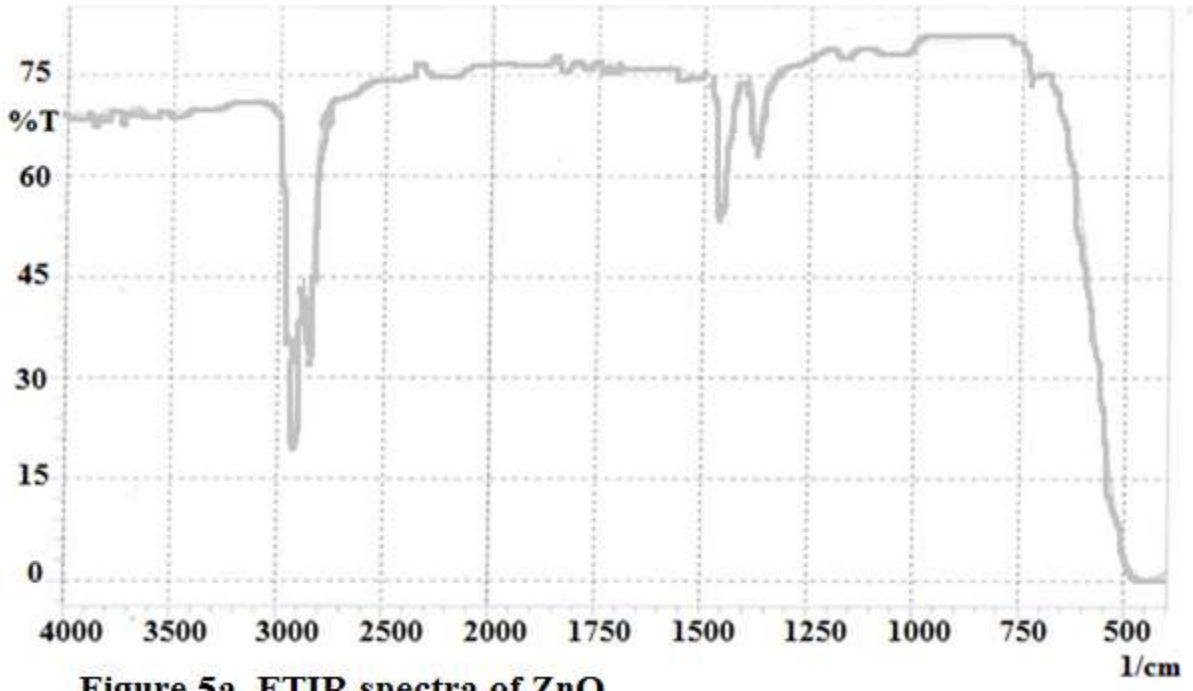

Figure 5a. FTIR spectra of ZnO

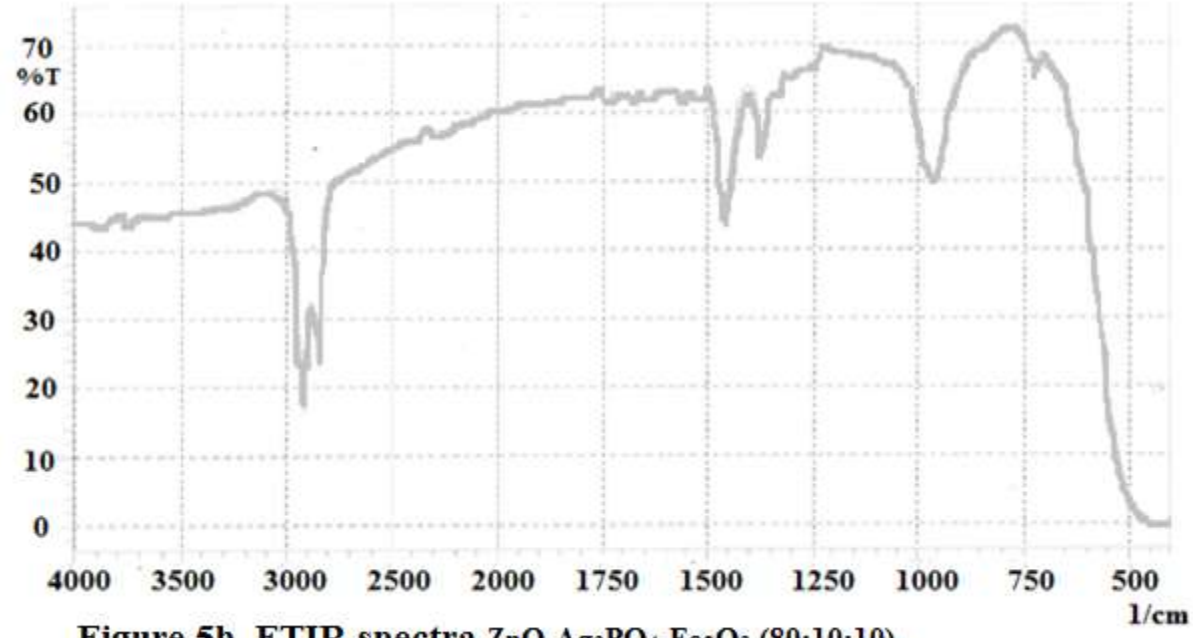

Figure 5b. FTIR spectra ZnO-Ag_3PO_4-Fe_2O_3 (80:10:10)

4.2. Photocatalytic Activity

4.2.1. Photocatalytic performance of ternary nanocomposite with different molar composition

The photocatytic performance of the synthesized ZnO-Ag_3PO_4-Fe_2O_3 photocatalyst in different molar compositions for the degradation of aqueous MB dye solution under visible light irradiation, with an initial dye concentration of 10 mg/L, catalyst load of 140 mg and solution pH of 6 was studied as a

function of irradiation time, and the results obtained as such are provided in Appendix Table 2. Accordingly, the plot of percentage degradation as a function of irradiation time (Figure 6) indicates that the maximum percentage degradation (90.7%) of the organic dye occurred at the ZnO-Ag_3PO_4-Fe_2O_3 photocatalyst molar composition of 80:10:10, respectively. Since the crystal size of photocatalyst (80:10:10) was lower with higher specific surface area among the nano-composite.

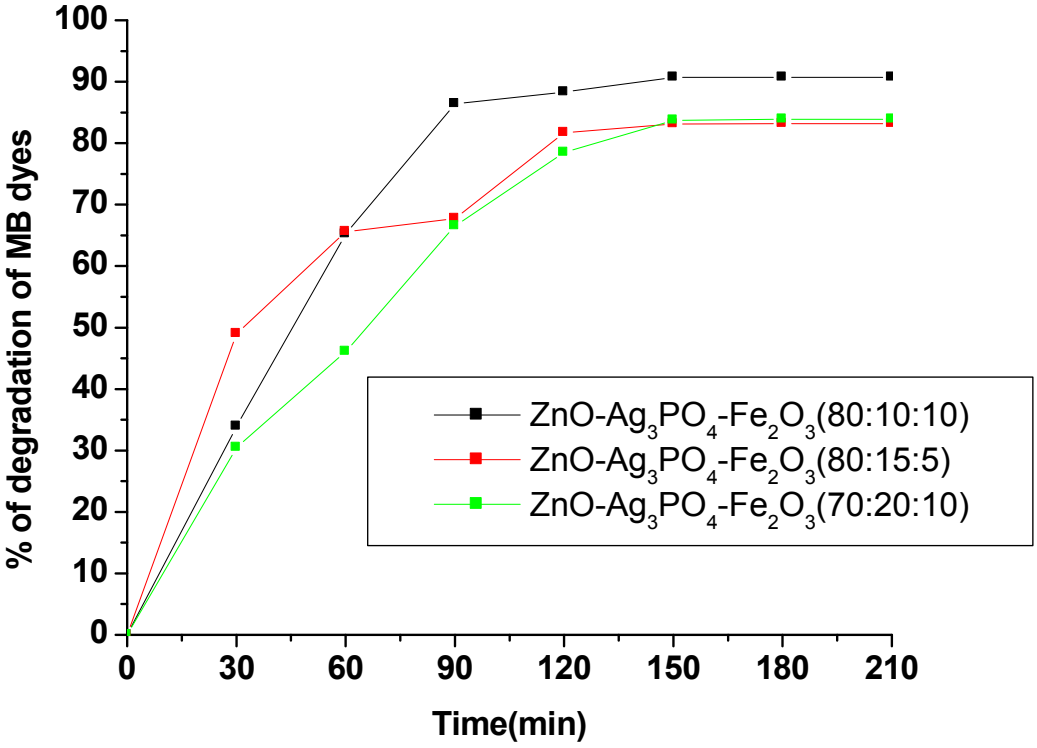

Figure 6. Plot of % degradation of as synthesized ZnO-Ag_3PO_4-Fe_2O_3 (80:15:5), ZnO:Ag_3PO_4:Fe_2O_3 (80:10:10), ZnO-Ag_3PO_4-Fe_2O_3 (70:20:10) nanocomposites under visible light irradiation. Using 10ppm of MB, pH 6, 50^oC and 140mg of the synthesized catalyst

4.2.2. **Photocatalytic Efficiency of ZnO-Ag_3PO_4-Fe_2O_3 (80:10:10) Photo-catalyst**

The photocatalytic degradation performances of various photocatalysts; ZnO, Ag_3PO4, ZnO-Ag_3PO_4-Fe_2O_3 (80:10:10), in the degradation of MB were evaluated using initial dye concentration of 10 mg/L and the catalyst load of 140 mg and 50 ^oC under visible light radiation. The percentage degradations of the dye by the photocatalyts after 150 min under visible light irradiations were found to be 34, 66 and 90% respectively as demonstrated in Figure 7 and Appendix Table 3.

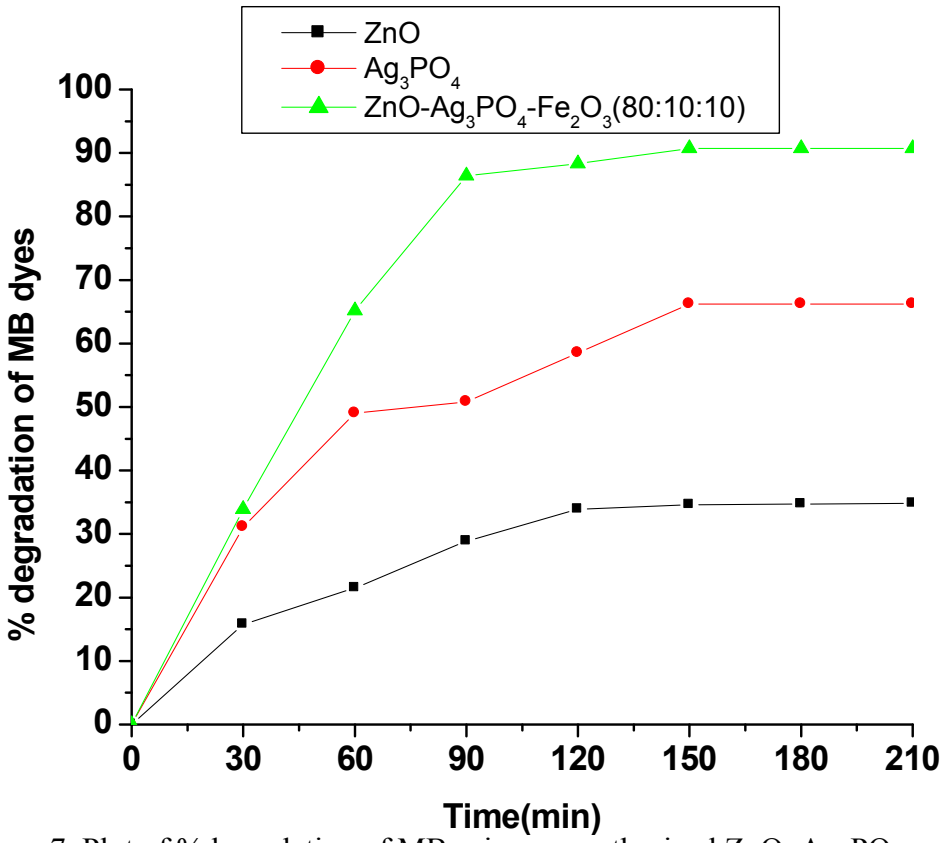

Figure 7. Plot of %degradation of MB using as synthesized ZnO, Ag_3PO_4 and ZnO-Ag_3PO_4-Fe_2O_3 (80:10:10) nanocomposites under visible light irradiation. Using 10 ppm of MB, pH 6, 50 ^oC and 140 mg of the synthesized catalyst

Using 10 ppm of MB, at 6 pH solution and 140 mg of synthesized catalyst under 50 ^oC ZnO demonstrated the lowest photocatalytic activity (34%) due to its wide band gap that makes it less sensitive to the visible portion of solar energy or that hinder the photocatalytic activity of ZnO [67].The degradation efficiency of Ag_3PO_4 (66%) is higher than that of ZnO; due to its narrow band gap which makes it able to harvest visible portion of the spectrum and it has better oxidizing power [68]. But, inherent photo-corrosion factors hamper its efficiency for effective utilization of visible light [69].This is possibly due to the fast recombination rate of e^- h^+ pairs [64]. In general, the coupling effect of narrow band gap photocatalysts with wide band gap counterpart increases light absorption of latter.

4.2.3. **Effect of the Solution pH**

To study the solution pH effect the experiments were conducted at pH 2, 4, 6, and 8 with initial dye concentration of 10 ppm and catalyst load of 140 mg as a function of irradiation time of 150 min the

results of which is indicated in Figure-8 and Appendix Table 6. The pH solution was adjust by adding NaOH, HCl acid and acetate and phosphate buffer solutions. Thus, the % degradation of MB was 52.2 at pH 2, 69.1 at pH 4,' 90.7 at pH 6 and 81.8 at pH 8 respectively. The results showed that the pH of solution had a direct influence on the heterogeneous photocatalysis process. As observed in Figure-10 and Appendix Table 6. This indicates the significant role of the surface properties of the selected ZnO-Ag_3PO_4-Fe_2O_3 (80:10:10) photocatalyst. Thus, it was clearly observed that the % degradation of MB dye on the surface of ZnO-Ag_3PO_4-Fe_2O_3 (80: 10:10) was found to increase with increasing the solution pH up to 6 then started to decrease above this optimum value. Thus, the acid base property of the as synthesized heterogeneous photocatalyst surface has considerable influence on the photocatalytic efficiency with varying pH. It can be observed from the graph in Figure -10 such that as the solution becomes more basic (higher pH), the photocatalytic degradation efficiency of the catalyst tends to decrease owing to the development of negative charge on the catalyst surface, which induces repulsion on the negatively charged dye molecules. In the contrary, the degradation of MB becomes even more hampered at lower pH (acidic) condition. This may be explained by the fact that the sorption of the MB on the catalyst surface is prevented because of the increased positive charges on the catalyst surface, which persuades repulsion on the positive charged dye molecules i.e. principle of ion-ion repulsion. It can be concluded that the maximum degradation efficiency (90.7%) was obtained at pH= 6, this was selected as optimum pH in the subsequent experiments.

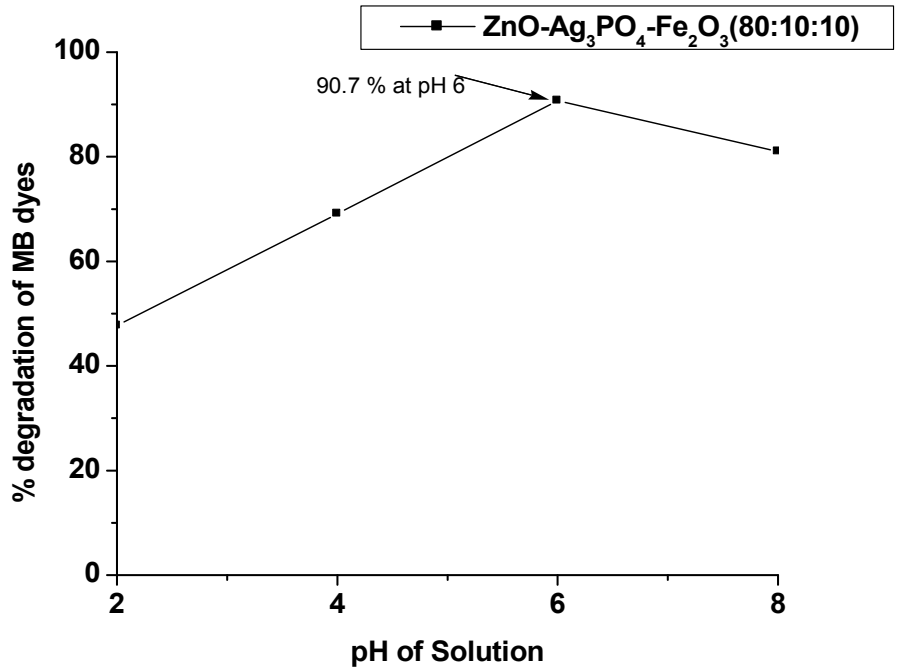

Figure 8. Plot % degradation of MB dyes at different pH of solutions after 150 minute visble light irradiation

4.2.4. **Effect of Catalyst dose**

The experiment was conducted by varying the concentration of the synthesized selected photocatalyst ZnO-Ag_3PO_4-Fe_2O_3 (80: 10:10) keeping pH at 6, dye concentration at 10 ppm and irradiation time of 150 min. The photocatalyst load was ranged from 100 mg to 160 mg. The results of this experiment are shown in Figure 9 and Appendix Table 4. Accordingly, the % degradation increased up to 140 mg then decreased, when we adding more than this dose. This observation may be explained in terms of restricted active sites on photocatalyst surface. Furthermore, it was reported that for a very high particle concentration the suspension turbidity increases. In this situation, the light penetration decreases, as a result of an enhanced light scattering effect, and consequently the photocatalaytic degradation becomes less effective [54]. A catalyst load of 140 mg is therefore selected as optimum value in the experiment following

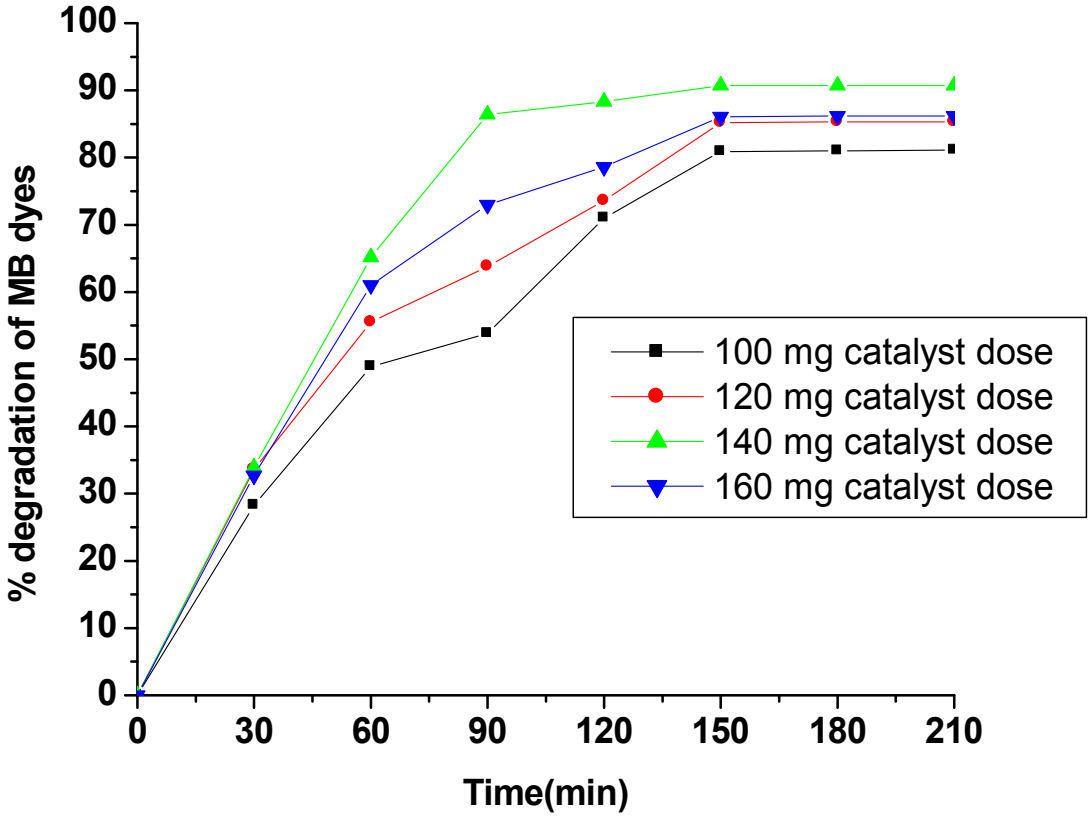

Figure 9. Plot of % Degradation of MB at different ZnO-Ag_3PO_4-Fe_2O_3 (80:10:10) catalyst load under visible irradiation keeping pH and dye concentration as constant. Catalyst load= 100mg, 120mg, 140mg and 160 mg, dye concentration= 10ppm at pH=6 under 50^oC.

4.2.5. **Effect of initial dye concentration**

The effect of initial dye concentration on the photocatalytic degradation efficiency was studied in the concentration range from 10 mg/L to 25 mg/L of MB solution. The other parameters such as catalyst dose and pH were kept at 6 and 140 mg under 50 ^{o}C respectively. The maximum degradation efficiency was obtained for the minimum dye concentration considered, which is 10 mg/L based on (Figure 12 and Appendix Table 8). Moreover, it was reported that the high concentration of pollutants in water saturates on the catalyst surface and hence reduces the photonic efficiency and deactivates the photocatalyst efficiency [70]. This reality helps us to think that there should be a maximum dye coverage allowing efficient reaction at the active sites. Above that, the dye gets inefficiently adsorbed preventing the interactions with photons of the light, thus resulting in a decrease of the photodegradation efficiency [61].

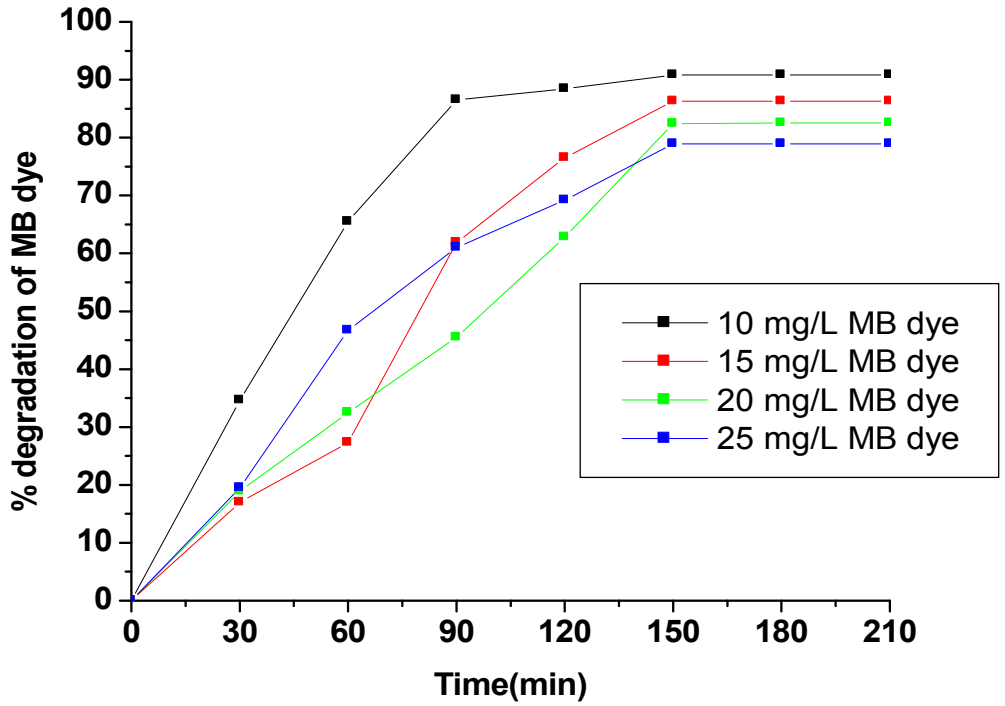

Figure 10. Plot % of degradation of MB dye under visible irradiation using ZnO-Ag_3PO_4-Fe_2O_3 (80:10:10) photocatalyst at different initial dye concentration. Catalyst load= 0.14g, at pH= 6.

4.2.6. **Effect of temperature**

The ZnO-Ag_3PO_4-Fe_2O_3 (80:10:10) ternary nanocomposite photocatalyst with 50 ^{o}C temperature shows higher photocatalytic activity than that of one with 25^{o}C. In addition, the degradation rates of

the methylene blue solution after 90, 120 and 150 min for the ZnO-Ag_3PO_4-Fe_2O_3(80:10:10) composite photocatalyst with 50 ^oC temperature are 86,88 and 90 % respectively, while the corresponding degradation rates for the ZnO-Ag_3PO_4-Fe_2O_3 (80:10:10) nanocomposite photocatalyst with 25 ^oC are 71, 76 and 82%. This may be due to the thermal motion of molecules accounting for the different temperatures for ZnO-Ag_3PO_4-Fe_2O_3 (80:10:10) ternary nano composite photocatalysts. When thermal energy increase in the photocatalyst surface the rate of electron hole pairs recombination also increase. Therefore the photocatalytic efficiency of the ZnO-Ag_3PO_4-Fe_2O_3 (80:10:10) nanocomposte is affected by high temperature.

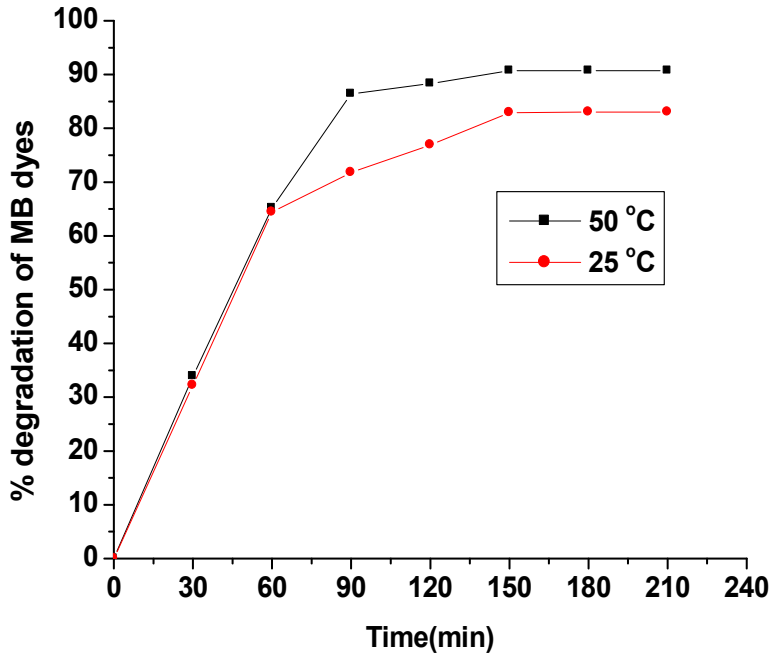

Figure 11. shows the effect of temperature for degradation MB by ZnO-Ag_3PO_4-Fe_2O_3 composite photocatalysts

4.2.7. **Recyclability of the Photocatalysts**

The ZnO-Ag_3PO_4-Fe_2O_3 (80:10:10) photocatalyst was evaluated the extent of recyclability as shown in Figure 12, and Appendix Table 5. In this experiment, we followed the same optimum operating conditions we employed for the ternary system ZnO-Ag_3PO_4-Fe_2O_3 (80:10:10) with initial dye concentration of 10 ppm, catalyst load of 140 mg , pH of 6, and irradiation time of 150 min. A small and gradual decrease in the activity of nanocatalyst was observed for the first two cycles to 90.7 and 85.5% respectively. However, a gradual decrease has been observed in photocatalytic degradation activities of ZnO-Ag_3PO_4-Fe_2O_3 (80:10:10) ternary nanocomposite for the last one cycle with

degradation efficiency of 81.0 % respectively. This experiment confirms the potential recyclability of the as synthesized ZnO-Ag_3PO_4-Fe_2O_3 (80:10:10) photocatalyst for three subsequent cycles with slight losing its efficiency. Therefore, the ZnO-Ag_3PO_4-Fe_2O_3 (80:10:10) acts as a stable photocatalyst with high efficiency.

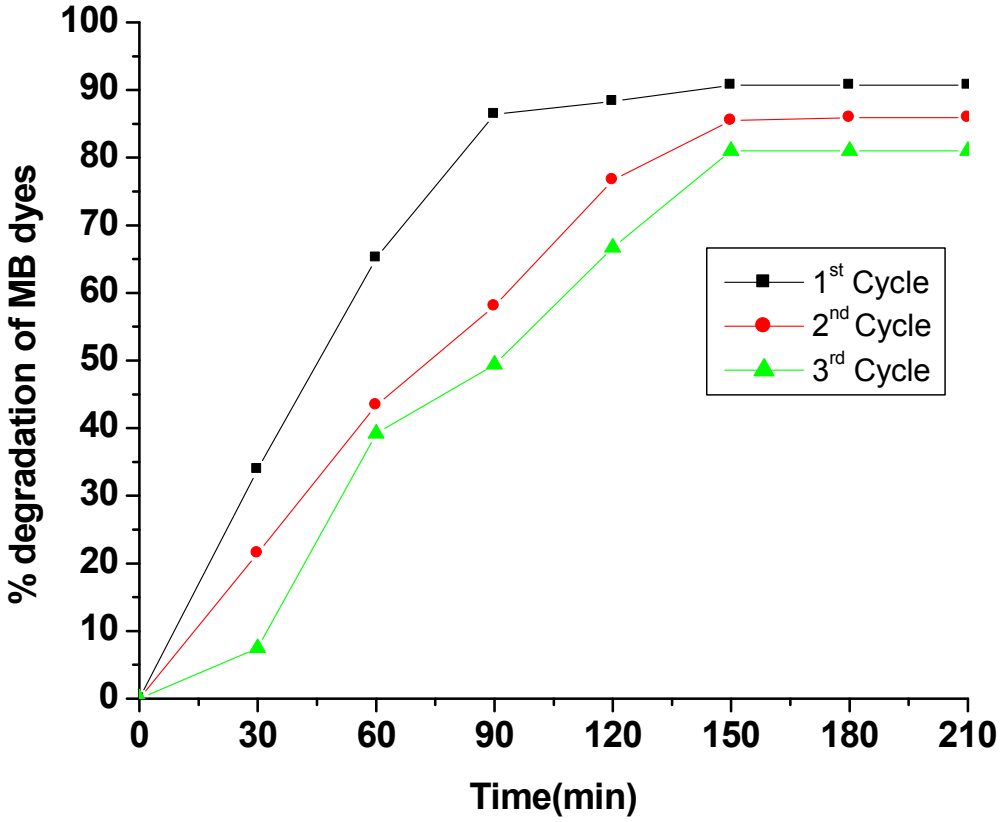

Figure 12. Plot of degradatio of MB dyes by ZnO-Ag_3PO_4-Fe_2O_3 (80:10:10) photocatalyst with recycle using over under visible irradiation. at PH= 6, Catalyst load= 0.14 g, initial dye concentration= 10ppm

4.2.8. **Real sample analysis**

Real sample from Addis Ababa Haile Garment Textile Industry sewage tanker was studied for its photo catalytic degradation of color. All liquid sewages from different department of the industry are collected together into swage tanker. The efficiency of the synthesized ZnO-Ag_3PO_4-Fe_2O_3 (80:10:10) ternary nanocomposite photocatalyst for the degradation of the real sample under visible light irradiation was studied as a function of irradiation time, and the results obtained as such are provided in Appendix Table 9.

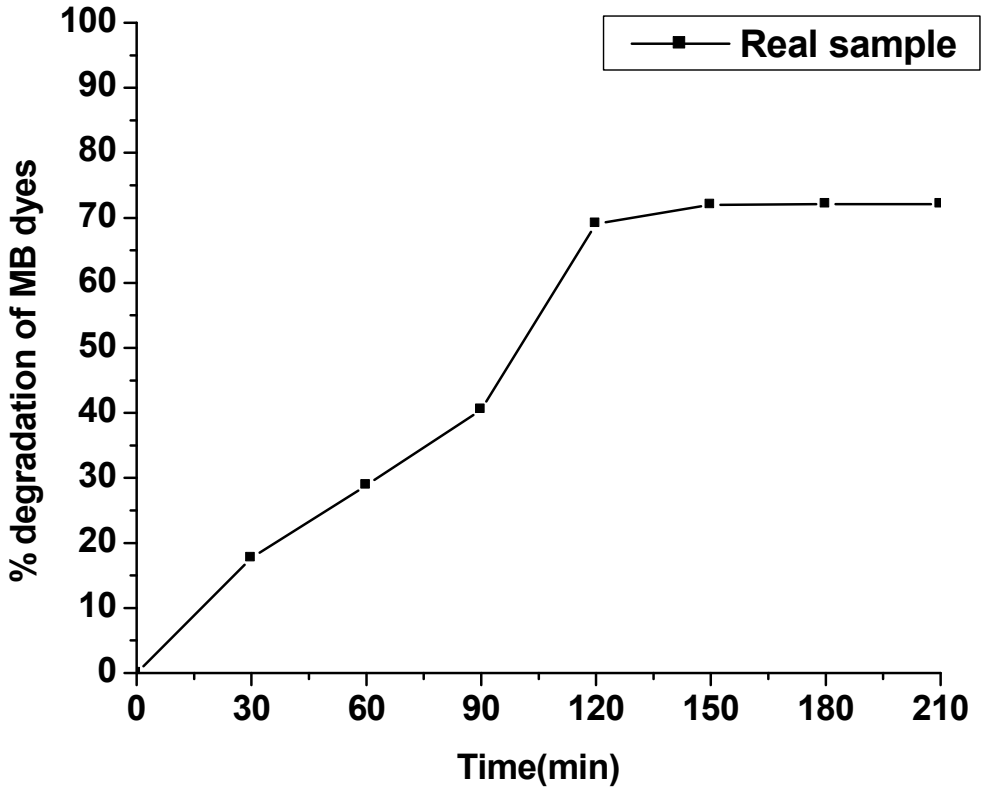

Figure 13. Plot of Percentage degradation of real sample sewage from Haile Garment Textile Industry swage tanker under visible irradiation using ZnO-Ag_3PO_4-Fe_2O_3 (80:10:10) photocatalyst

Accordingly, the plots of percentage degradation as a function of irradiation time depicted in Figure 13 indicates that percentage degradation (72%) of the real sample occurred at the ZnO-Ag_3PO_4-Fe_2O_3 (80:10:10) ternary nanocomposite at pH=6, 140 mg catalyst dose and 50 ^oC photocatalyst under 150 minute visible light irradiation.

5. CONCLUSIONS AND RECOMMENDATIONS

5.1. Conclusions

ZnO, Ag_3PO_4 nanoparticle and ZnO-Ag_3PO_4-Fe_2O_3 ternary nano comoposite were synthesized by precipitation method using aqueous solutions of Zn $(NO_3)_2.6H_2O$, Na_2CO_3, $AgNO_3$, $Na_2HPO_4.2H_2O$ and $Fe(NO_3)_2.9H_2O$ respectively. The particle size, crystal structures, band gap energy, bond vibration (stretching) and optical properties of all the as synthesized photocatalysts were performed using X-ray diffiraction (XRD), single beam UV-Vis and FTIR analytical techniques respectively. The XRD result in the ZnO-Ag_3PO_4-Fe_2O_3 (80:10:10) ternary nanocomposite shows hexagonal wurtzite structure of ZnO, body centered cubic structure of Ag_3PO_4 and hexagonal crystal structure α-Fe_2O_3 crystal structures. The calculated band gap of the narrowest ZnO-Ag_3PO_4-Fe_2O_3 ternary nanocomposite is about 2.34 eV that obtain from UV-Vis spectra data. Photocatalytic activities of the as synthesized nanoparticles and nanocomposite were investigated on the target pollutant MB dyes under visible light irradiation. Key parameters of effect of concentration of dye, catalyst dose, pH of solution, effect of temperature and irradiation time have important effects on the photocatalytic activity of the ZnO, Ag_3PO_4 nanoparticle and ZnO-Ag_3PO_4-Fe_2O_3 (80:10:10) ternary nano comoposite photocatalysts. The degradation rate of ZnO, Ag_3PO_4 nanoparticle and ZnO-Ag_3PO_4-Fe_2O_3 ternary nano comoposite is close to 34%, 66% and 91%. The ternary system ZnO-Ag_3PO_4-Fe_2O_3 (80:10:10) nanocomposite was achieved high photocatalytic efficiency at 150 minute visible light irradiation time, at pH 6, at 50 ^oC temperature, at 10 mg/L MB dye concentration, at 140 mg catalyst dose and first cycle using catalyst optimum operational parameters. The real swage sample also degraded about 72 % with all optimum operation parameters. All the results confirmed that the photocatalytic activities of ZnO-Ag_3PO_4-Fe_2O_3 ternary nano comoposite, was comparatively higher than ZnO and Ag_3PO_4 photocatalysts. The results showed that the prepared ZnO-Ag_3PO_4-Fe_2O_3 (80:10:10) ternary nanocomposite photocatalysts have presented a huge potential application in wastewater treatment.

5.2. **Recommendations**

ZnO-Ag_3PO_4-Fe_2O_3 (80:10:10) nano-composite synthesis, characterization, photocatalytic and applications is studied in this work. Therefore, the author recommends researchers to pay attention for advancing further research on this particular area. And the researchers should be characterized the synthesis product by additional instruments such as SEM and TEM to help the particles are nano or not by comparing with the XRD data. Looking for other polymeric or inorganic supports to immobilize the ternary system to enhance the efficiency, attempt potential application in the area of sensors, solar cells, super capacitors, fuel cells, antimicrobial etc, try other synthetic approaches to fabricate ternary system with controlled size and better morphology. Involve photocatalytic parameters such calcination temperature, and time as well as intensity of light etc. are among many other important factors that should be given equal attention by further research works to lift the efficiency even better.

REFERENCES

[1]. Tsuboy, M.S.; Angeli, J.P.F.; Mantovani, M.S.; Knasmüller, S.; Umbuzeiro, G.A.; Ribeiro, L.R. Genotoxic, mutagenic and cytotoxic effects of the commercial dye CI Disperse Blue 291 in the human hepatic cell line HepG2. *Toxicol. in Vitro.* **2007**, *21*, 1650-1655.

[2]. Tang, W, Z, and H, An. Photocatalytic degradation of kinetics and mechanism of acid blue 40 by TiO_2 /Vis in aqueous solution.*Chemsphere.* **1995**, 31, 4171-4183.

[3]. Hoffmann, M.R.; S.T.Martin, W.Choi and D.W.Bahnemann. Environmental applications of semi-conductors photocatalysis.*Chem.Rev*. **1995**, 95, 69-96.

[4]. Wang, H.; S. Baek, J. Lee and S. Lim. High photocatalytic activity of silver-loaded ZnO-SnO_2 coupled catalysts. *Journal of Environmental Chemical Engineering.*. **2009**, *146, 355-361.*

[5]. Haileyesus, Tedla.; Isabel, Diaz.; Tesfahun, Kebede.; Abi M, Taddesse. Synthesis, characterization and photocatalytic activity of zeolite supported $ZnO/Fe_2O_3/MnO_2$ nanocomposite. *Journal of Environmental Chemical Engineering.* **2015**, 3, 1586-1591.

[6]. Hu, C.; Lan, Y. J.; Qu, X. Hu. and Wang, A. $Ag/AgBr/TiO_2$ visible light photocatlyst for azo dye bacteria. *Journal Physical chemistry*. **2006**,110, 4066-4072.

[7]. Wang, Z.; Cai, W.; Hong, X.; Zhao, X.; Xu, F. and Cai, C. Photocatalytic degradation of phenol in aqueous nitrogen-doped TiO_2 suspension with various light sources. *Journal Applied Catalysis.* **2005**, 57, 223-231.

[8]. He,H.Y.;J.F. Hung.L.Y.; Cao, and J.P.Wu. photodegradiation of methyl orange aqueous on $MnWO_4$ powder under different lightbresources and intial PH. *Desalination.* **2010**, 252, 149-159.

[9]. Karásková, K.; Z. Chromcáková, S. Studentová, V. Matejkab, K. Jirátová , and L. Obalová. A comparative study of TiO_2-supported and bulk Co-Mn-Al catalysts for N_2O decomposition. *Catal. Today*. **2012**, 4, 7931.

[10]. Wang,Y.Q.; GU, B. and Xu, W.L. Electrocatalytic degradation of phenol on several metal oxide anodes. *Journal Hazardous Materials.* **2009**,162, 1159-1164.

[11]. Zhang, J.; Bi, H.; He, G.; Zhou, Y and Chen, H. Fabrication of Ag_3PO_4-PANI-GO composites with high visible light photocatalytic performance and stability. *Journal of Environmental Chemical Engineering.* **2014**, 2, 952-957.

[12]. Bi, Y; Ouyang, S; Umezawa, N; Cao J and Ye J. Facet effect of single-crystalline Ag_3PO_4 sub-microcrystals on photocatalytic properties. *Journal of the American Chemical Society*. **2011**, 133(17), 6490-6492.

[13]. Xu, YS and Zhang, WD. Monodispersed Ag_3PO_4 nanocrystals loaded on the surface of spherical Bi_2MoO_6 with enhanced photocatalytic performance. *Dalton Transactions*. **2013**, 42(4), 1094-1101.

[14]. Zhang, L; Zhang, H; Huang, H; Liu Y and Kang Z. Ag_3PO_4/SnO_2 semiconductor nanocomposites with enhanced photocatalytic activity and stability. *New Journal of Chemistry*. **2012**, 36(8), 1541.

[15]. Li, G and Mao, L. Magnetically separable Fe_3O_4-Ag_3PO_4 submicrometre composite: facile synthesis, high visible light-driven photocatalytic efficiency, and good recyclability. *RSC Advances*. **2012**, 2(12), 5108.

[16]. Ewais, E.; M. Hessien, and El-Geassy. In-Siut synthesis of Magnatic Mn-Zn Ferrite Ceramic objects by solid state reaction. *Australi Ceram. Soci.* **2008**, 44, 57-62.

[17]. Liotta, L.F.; M. Gruttadauria, G. Di Carlo, G. Perrini, V. Librando. Heterogeneous catalytic degradation of phenolic substrates: Catalysts activity, *Journal of Hazardous Materials*, **2009**,162 (3), 588-606.

[18]. Shawabkeh, R. A.; O. A. Khashman, G. I. Bisharat,. Photocatalytic Degradation of Phenol using Fe-TiO2 by Different Illumination Sources, *International Journal of Chemistry*. **2010**, 2, (2), 10-18.

[19]. Lovestam. H. Rauscher; G. Roebben, B.S. Kluttgen; N. Gibson, J. Putaud and H. Stamm. Heterogeneous photochemical electron transfer, CRC Press, Boca, Raton and Florida, Luminescence. *Journal of Drug Delivery and Current Medicinal Chemistry.* **2010,** 17, 585-594.

[20]. Galoppini,E.;Rochford, J.;Chen,H.;Sraf,G.L.Y.;Hagfeldt,A. and Bschloo,G. Fast electron transport in metal organic vapor depostionn grown dy-sentized ZnO nanorod solar cells. *Journal Physical Chemistry.* **2006**, 110(33), 16159-16161.

[21]. Zhen, M and Francisco, Z, **2006**. Heterogeneous Catalysis by Metals in Encyclopedia of Inorganic Chemistry.

[22]. Height, M.J.; Pratsinis, S.E.; Mekasu, Wandumrong, O. and Praserthdam, P, .Ag-ZnO catalysts for Uv-photodegradation of Methylene blue. *Applied Catalysis.B; Environment*. **2006**, 63, 305-3112.

[23]. Tai,C.; Gu, X. X.; Zou, H.; and Guo, Q.H. A new simple and sensitive fluorometric method for the determination of hydroxyl radical and its application. *Talanta.* **2002**, 58, 661.

[24]. Pera-Titus, M.; Garcia-Molina, V.; Banos, M.A.; Gimenez, J. and Esplugas, S. Degradation of chlorophenols by means of advanced oxidation processes: a general review. *Applied Catalysis Environmental.* **2004**, 47(4), 219-225.

[25]. Garcia-Montano,J.; Perez-Estrada,L.; Oller, I.; Maldonado, M. I.;Torrades, F. and Peral, J. Pilot plant scale reactive dyes degradation by solar photo-fenton and biological processes *Journal of Photochemical and Photobiologcal part A*. **2008**,195, 202-205.

[26]. Akram, M.; Kanwal, Z.; Rauf, A.; Sabri, N.; Riaz, S. and Naseem, S. Size and shapedependent antibacterial studies of silver nanoparticles synthesized by wet chemical routes. Journal of *Nano science.* **2016**, 6, 74.

[27]. Schwitzgebel, J.; Ekerdt ,JG.; Gerischer, H. and Heller, A. Role of the oxygen molecule and of the photogenerated electron in TiO_2 photocatalyzed Air oxidation reactions. *Journal of Physical Chemistry.* **1995**, 99, 5633-5638.

[28]. Xiong ,S.; George ,S.; Ji Z, Lin S.; Yu H, Damoiseaux R; France B.; Ng KW. and Loo SCJ. Size of TiO_2Nanoparticles Influences their Phototoxicity: An in Vitro Investigation. *Archives of Toxicology.* **2013**, 87, 99-109.

[29]. Zhang, F.; Jin, J.; Zhong, X.; Li, S.; Niu, J.; Li, R.; Ma, J, Pd immobilized on Amine functionalized magnetite nanoparticles: A novel and highly active catalyst for hydrogenation and Heck reactions. *Green Chemistry.* **2011**,13, 1238-1243.

[30]. Linsebigler, A.L.; Lu, G. Q. and Yates, J. T. Photocatalysis on TiO_2 surfaces-principles: Mechanisms and Selected results. *Chemical Review.***1995**, 95, 735-758.

[31]. Herrman, J.M. Hetrogenenous photocatalysis: fundamentals and applications to the removal of various types of aqueous pollutants.*Catalysis Today*.**1999**, 53,115-129.

[32]. Hoffmann,M.; R, Martin, S. T.; Choi, W. and Bahnemann, D. W. Environmental applications of semiconductor photocatalysis. *Chemical Review,* **1995**, 95(1), 69-78.

[33]. Bessa, E.; Sant, Anna.; Jr ,G L. and Dezotti, M. Photocatalytic/H_2O_2 treatment of oil field produced waters. *Applied Catalysis B: Environmental.* **2000***,* 29, 125-134.

[34]. Li, J.H.; Shen, D.Z.; Zhang, J.Y.; Zhao, D.X.; Li, B.S.; Liu,Y.C. and Fan, X.W. The effect of Mn^{2+} doping on the structure and photoluminescence of ZnO nano films. Synthesized by sol-gel method. *Chinese Journal of Catalysis.* **2007**,352, 122-123.

[35]. Height, M.J.; Pratsinis, S.E.; Mekasu, Wandumrong, O. and Praserthdam, P, .Ag-ZnO catalysts for Uv-photodegradation of Methylene blue. *Applied Catalysis.B; Environment*. **2006**, 63, 305-3112.

[36]. Hsiu-Fen, Lin.; Shih-Chieh, Liao. and Chen-Ti, Hu. A new approach to synthesize ZnO nanoparticles with DC thermal plasma technique. *Journal of Crystal growth.* **2009**, 311, 1378- 1384.

[37]. So-Jung, kim and Dong-Wha park. Preparation of ZnO nano poweders by thermal plasm and characterization of photocatalytic property. *Applied surface Science*. **2009**,255, 5363-5367.

[38]. Kamat,P.V**.** Electrocatalytically active graphene-platinum nanocomposites. *Chemistry of Pearson Education.***1993***,* 93, 267-300.

[39]. Choi, W.Y.; Termin, A. and Hoffmann, M.R. Role of metal-ion dopants in quantum sized TiO_2-Correlation between photo reactivity and charge-carrier recombination dynamics. *Journal of Physical Chemistry.* **1994**, 98, 13669-13679.

[40]. Wang, C.M.; Heller, A. and Gerischer, H**.** Environmental applications of semiconductor Photocatalysis**.** *Journal of the American Chemical Society.* **1992**,114, 5230-5234.

[41]. Yi.Z.G, J.H. Ye, N. Kikugawa, T. Kako, S.X. OuYang, H. Stuart-Williams, H. Yang,J.Y. Cao,W.J. Luo, Z.S. Li, Y. Liu, R.L.Material Research bulletin. *Withers, Nat. Mater.* **2010**, 9, 559.

[42]. Tiwana, P.; Docampo, P.; Johnston,M.B.; Snaith,H.J.; Herz,L.M.; . Electron mobility and injection dynamics in mesoporous ZnO, SnO_2, and TiO_2 films used in dye-sensitized solar cells. *Journal American Chemical Society nano* ACS. **2011**,**5***,* 5158-5166.

[43]. Wang, H.; S. Baek, J. Lee and S. Lim. High photocatalytic activity of silver-loaded ZnO-SnO_2 coupled catalysts. *J. Chem. Eng.* **2009**, *146, 355-361.*

[44]. K. M. Parida, S. S. Dash and D. P. Das. 'Physico-chemical characterization and Photo-catalytic activity of zinc oxide prepared by various methods', J. Colloid Interface Sci., **2006**, 298, 787–793.

[45]. Dhar, S. Formation, dynamics, and characterization of nanostructures by ion beam irradiation.*Critical Reviews in Solid State and Materials Sciences*. **2007**, 32(1), 1–50.

[46] J. X. Wang; X. W. Sun, Y. Yang; H. Huang, Y. C. Lee, O. K. Tan and L. Vayssieres: 'Hydrothermally grown oriented ZnO nanorod arrays for gas sensing applications', Nanotechnology, **2006**, 17,4995–4998.

[47]. Zhen, M and Francisco, Z, 2006. Heterogeneous Catalysis by Metals in Encyclopedia of Inorganic Chemistry, John Wiley. doi:10.1002/0470862106.ia084.

[48]. Munnik, P.; Petra, E. de Jongh, and Krijn P. *de Jong- inorganic Chemistry Review.* **2015**, 115,6687-671.

[49]. Korotcenkov, G. The role of morphology and crystallographic structure of metal oxides in response of conductometric-type gas sensors. *Materials Science and Engineering.* **2008**. 61, 1-39.

[50]. Ece . Modern methods for rapid X-ray diffraction data collection from crystals of macromolecules. *Methods in Molecularbiology.* **2012**, 56, 87-126.

[51]. Chong M.N.; Jin B., Chow C.W.K., Saint C. Recent developments in photocatalytic water Treatment Technology: *A Review. Water Resources.* **2010**, 44, 2997-3027.

[52]. Kosmulski, M. pH-dependent surface charging and points of zero charge: III. Update. *Journal of Colloid Interface Science.* **2006**, 298, 730-741.

[53]. Sun, J.; Wang, S.; Sun, J.; Sun, R., Sun, S. and Qiao, L. Photocatalyticdegradation and kinetics of orange G using nano sized Sn(IV)/TiO_2/AC photocatalyst. *Journal of Molecular Catalysis A: Chemical.* **2006**,260, 241-246.

[54]. Mohammad, A.; Abdolhamid, H.; Askarpour, A.; Zaydabadi, M. Synthesis, characterization, and application of MgO/ZnO nanocomposite supported on activated carbon for Photocatalytic degradation of methylene blue. *Research Chemistry Intermed* **2015**, 41,6157-6168.

[55]. Chong M.N.; Lei S.; Jin B.; Saint C.; Chow C.W.K. Optimization of an annular photo reacts or process for degradation of congored using a newly synthesized titania impregnated kaolinite nano-photocatalyst.*Separation and Purification Technology.* **2009**, 67, 355-363.

[56]. Gaya U.I.; Abdullah A.H. Heterogeneous Photocatalytic Degradation of Organic Contaminants over Titanium Dioxide: A Review of Fundamentals, Progress and Problems. *Journal of Photochemistry and Photobiology C Photochemistry Reviews.* **2008**, 9, 1-12.

[57]. Bhatkhnade, D.; S, Kamble, S,P.; Sawant S,B. and Pangarkar,V. Photocatalytic and photo chemical degradation of nitro benzene using artificial ultraviolet light. *Journal of Chemical Engineering.* **2004**,102, 283-290.

[58]. Houas, H.; Lachheb, M.;Ksibi, E.; Elaloui, C.; Guillard, J. M.; Cao, P.X.; Shao,Y. and Zhen Anew perspective for effect of Bi on the photo catalytic activity of Bi dopedTiO_2 *Applied ca talysis B: Journal of Environmental Science*. **2011**,125, 294-303.

[59]. Chen, L.C.; Huang, C.M.; and Tsai, F.R. Characterization and photocatalytic activity of K^+ doped titanium oxide photocatalysts. *Journal Molecular Catalysis.* **2008**,265, 133-140.

[60]. Hong, R.Y.; J.H. Li, L.; Chen, D.Q.; Liu, H.Z.; Li, Y.; Zheng. S and Ding, J. Synthesis, surface modification and photo catalytic property of ZnO nanoparticles. *Powder Technology.* **2009**,189, 426-432.

[61]. Kai Huanga; Yaohui Lva; Wei Zhanga; Shanyun Suna; Bin Yanga; Fangli Chia; Songlin Rana and Xianguo Liua. One-step Synthesis of Ag_3PO_4/Ag Photocatalyst with Visible-light Photocatalytic Activity School of *Materials Science and Engineering, Anhui Key Laboratory of Metal Materials and Processing, Anhui University of Technology China*. **2015**, 18(5), 940-943.

[62]. Salimi, F.; Abdollahifar,M.; Jafari, P. and Hidaryan,M. A new approach to synthesis and growth of AlOOH nanocrystalline with high pore volume. *Journal of the SerbiaChemical Society,* **2017**, 82, 1-11.

[63]. Akram, M.; Kanwal, Z.; Rauf, A.; Sabri, N.; Riaz, S. and Naseem, S. **2016**. Size and shape dependent antibacterial studies of silver nanoparticles synthesized by wet chemica routes.*Nanomaterials*6, 74; doi: 10.3390/nano6040074.

[64]. Liu, L.; Lv, J.; Xu, G.; Wang, Y.; Xie, K. Chen, Z.; Wu, Y. Uniformly dispersed CdS nano particle sensitized TiO_2 nanotube arrays with enhanced visible-light photocatalytic activity and stability. *Journal of Solid State Chemistry,* **2013**, 208, 27-34.

[65]. Tofik, A.S.; Abi M, Taddesse., Tesfahun, K.T. and Girma, G. Fe-Al binary oxide nanosorbent: synthesis, characterization and phosphate sorption property.*Journal of Environmental Chemical Engineering,* **2016**,4, 2458-2468.

[66]. Ahmed,F.; Kumar,S.; Arshi,N.; Anwar, M.S.; Su-Yeon, L.; Sukil, G.; Wonpark, D.; Koo, B.H.; Lee, C.G. Preparation and characterizations of polyaniline (PANI)/ZnO nanocomposites film using solution casting method.*Thin Solid Films,* **2011**, 519, 8375-837.

[67]. Liu, J.; Zhu, K., Sheng, B.; Li, Z.; Tai, G.; Qiu, J.; Wang, J.; Chen, J.; You, Y.; Gu, Q.; Liu, P, Low temperature solid state synthesis and optical properties of ZnO/CdS nano composites. *Journal of Alloys and Compounds,* **2015**, 618, 67-72.

[68]. Wang,Yunfang.; Li, Xiuli.; Wang, Yawen.; Fan, Caimei. Novel visible-light AgBr/Ag_3PO_4 hybrids photocatalysts with surface plasma resonance effects. *Journal of Solid State Chemistry.* **2013**, 202, 51-56.

[69]. Zhang, J.; Bi, H., He, G.; Zhou, Y.; Chen, H. Fabrication of Ag_3PO_4−PANI−GO composites with high visible light photocatalytic performance and stability.*Journal of Environmental Chemical Engineering.* **2014**, 2, 952-957.

[70]. Saquib,M. and Muneer, M. TiO_2 mediated photocatalytic degradation of triphenyl methane dye (gentian violet), in aqueous suspensions. *Dyes and Pigments.* **2003**, 56, 37-49

[71]. López, R. and R. Gómez. Band-gap energy estimation from diffuse reflectance measurements on sol–gel and commercial TiO_2: a comparative study. *Journal of sol-gel science and technology*. **2012**, 61(1), 1-7.

APPENDICES

Appendix Table 1. UV-Vis spectra of appearance of ZnO, Ag_3PO_4 and ZnO-Ag_3PO_4-Fe_2O_3 (80:10:10) ternary nanocomposte by Ethanol and distill water ratio solvent.

ZnO (2ml ethanol:3ml distill water)		Ag_3PO_4 (1ml ethanol:4ml distill water)		ZnO-Ag_3PO_4-Fe_2O_3 (80:10:10) (4ml ethanol:6ml distill water)	
λ_{max}	Abs	λ_{max}	Abs	λ_{max}	Abs
300	2.401	300	2.107	300	1.691
306	2.31	306	1. 821	306	1.534
310	2.04	310	1. 743	310	1.486
320	1.87	320	1.686	320	1.403
325	1.745	325	1.595	325	1.388
351	1.618	351	1.557	351	1.351
363	1.724	363	1.546	363	1.29
374	1.909	374	1.529	374	1.261
377	1.996	377	1.521	377	1.253
385	1.88	385	1.501	385	1.246
390	1.789	390	1.499	390	1.235
410	1.673	410	1.493	410	1.288
434	1.613	434	1.605	434	1.293
448	1.508	448	1.61	448	1.324
460	1.49	460	1.631	460	1.341
480	1.376	480	1.648	480	1.392
512	1.248	512	1.813	512	1.409
530	1.213	530	1.601	530	1.587
550	1.199	550	1.512	550	1.216
570	1.167	570	1.485	570	1.088
600	1.123	600	1.424	600	1.041
650	1.106	650	1.39	650	1.004
700	1.089	700	1.261	700	0.962

Appendix Table 2. % degradation of as synthesized ZnO-Ag_3PO_4-Fe_2O_3 (80:15:5), ZnO-Ag_3PO_4-Fe_2O_3 (80:10:10), ZnO-Ag_3PO_4-Fe_2O_3 (70:20:10) nanocomposites under visible light irradiation. Using 10 ppm of MB, pH 6, 50 ^oC and 140 mg

ZnO-Ag_3PO_4-Fe_2O_3 (80:10:10)			**ZnO-Ag_3PO_4-Fe_2O_3 (80:15:5)**			**ZnO-Ag_3PO_4-Fe_2O_3 (70:20:10)**		
Time	Absorbance	%	Time	Absorbance	%	Time	absorbance	%
0	1.041	0	0	1.041	0	0	1.041	0
30	0.688	33.9	30	0.53	49	30	0.723	30.5
60	0.362	65.2	60	0.358	65.6	60	0.561	46.1
90	0.141	86.4	90	0.336	67.7	90	0.348	66.5
120	0.121	88.3	120	0.209	81.7	120	0.223	78.5
150	0.096	90.7	150	0.175	83.1	150	0.169	83.7
180	0.095	90.7	180	0.174	83.2	180	0.167	83.9
210	0.095	90.7	210	0.174	83.2	210	0.167	83.9

Appendix Table 3. % degradation of MB using as synthesized ZnO, Ag_3PO_4 and ZnO-Ag_3PO_4-Fe_2O_3 (80:10:10) nanocomposites under visible light irradiation using 10 ppm of MB, pH 6, 50 ^oC and 140 mg of the synthesized catalyst

ZnO			**Ag_3PO_4**			**ZnO-Ag_3PO_4-Fe_2O_3 (80:10:10)**		
Time	Absorbance	%	Time	Absorbance	%	Time	Absorbance	%
0	1.041	0	0	1.041	0	0	1.041	0
30	0.876	15.8	30	0.717	31.1	30	0.688	33.9
60	0.817	21.5	60	0.53	49	60	0.362	65.2
90	0.74	28.9	90	0.512	50.8	90	0.141	86.4
120	0.688	33.9	120	0.431	58.5	120	0.121	88.3
150	0.680	34.6	150	0.351	66.2	150	0.096	90.7
180	0.679	34.7	180	0.351	66.2	180	0.095	90.7
210	0.678	34.8	210	0.351	66.2	210	0.095	90.7

Appendix Table 4. % Degradation of MB at different ZnO-Ag_3PO_4-Fe_2O_3 (80:10:10) catalyst load under visible irradiation keeping pH and dye concentration as constant. Catalyst load= 100 mg, 120 mg, 140 mg and 160 mg, dye concentration= 10 ppm at pH=6 under 50 ^oC.

	100 mg			**120 mg**			**140 mg**			**160 mg**	
Time	Abs.	%	Time	Abs.	%	Time	Abs.	%	Time	Abs.	%
0	1.041	0	0	1.041	0	0	1.041	0	0	1.041	0
30	0.746	28.3	30	0.691	33.6	30	0.688	33.9	30	0.7	32.7
60	0.532	48.9	60	0.463	55.5	60	0.362	65.2	60	0.405	61
90	0.48	53.8	90	0.376	63.8	90	0.141	86.4	90	0.281	73
120	0.301	71	120	0.274	73.6	120	0.121	88.3	120	0.222	78.6
150	0.198	80.9	150	0.154	85.2	150	0.096	90.7	150	0.144	86.1
180	0.197	81	180	0.153	85.3	180	0.095	90.7	180	0.143	86.2
210	0.196	81.1	210	0.153	85.3	210	0.95	90.7	210	0.143	86.2

Appendix Table 5. Plot of ZnO-Ag_3PO_4-Fe_2O_3 (80:10:10) photocatalyst recycle using over MB dye under visible irradiation at PH= 6, Catalyst load= 0.14 g, initial dye concentration= 10ppm

	1st cycle			**2nd cycle**			**3rd cycle**	
Time	Absorbance	%	Time	Absorbance	%	Time	Absorbance	%
0	1.041	0	0	1.041	0	0	1.041	0
30	0.688	33.9	30	0.817	21.5	30	0.962	7.5
60	0.362	65.2	60	0.589	43.4	60	0.632	39.2
90	0.141	86.4	90	0.437	58	90	0.526	49.4
120	0.121	88.3	120	0.242	76.7	120	0.346	66.7
150	0.096	90.7	150	0.147	85.5	150	0.197	81.0
180	0.095	90.7	180	0.146	85.9	180	0.197	81.0
210	0.095	90.7	210	0.146	85.9	210	0.197	81.0

Appendix Table 6. % Degradation of MB by ZnO-Ag_3PO_4-Fe_2O_3 (80:10:10) photo-catalyst at different pH under visible irradiation keeping catalyst load and dye concentration as constant. Catalyst load= 0.14 g, dye concentration= 10 ppm and under 50 ^oC.

	pH 2			**pH 4**			**pH 6**			**pH 8**	
Time	Abs.	%	Time	Abs.	%	Time	Abs.	%	Time	Abs,	%
0	1.041	0	0	1.041	0	0	1.041	0	0	1.041	0
30	0.927	10.9	30	0.889	14.6	30	0.688	33.9	30	0.705	32.2
60	0.758	27.1	60	0.611	41.3	60	0.362	65.2	60	0.56	46.2
90	0.699	32.8	90	0.453	56.4	90	0.141	86.4	90	0.37	64.4
120	0.609	41.4	120	0.357	65.7	120	0.121	88.3	120	0.293	71.8
150	0.545	47.7	150	0.321	69.1	150	0.096	90.7	150	0.189	81.8
180	0.544	47.7	180	0.320	69.2	180	0.095	90.7	180	0.188	81.9
210	0.544	47.7	210	0.320	69.2	210	0.095	90.7	210	0.188	81.9

Appendix Table 7. % Degradation of MB by ZnO-Ag_3PO_4-Fe_2O_3 (80:10:10) photocatalyst at different temperature under visible irradiation keeping catalyst load and dye concentration as constant. pH=6

	50 ^oC			**25 ^oC**	
Time(min)	Abs.	%	Time.	Abs.	%
0	1.041	0	0	1.041	0
30	0.688	33.9	30	0.705	32.2
60	0.362	65.2	60	0.37	64.4
90	0.141	86.4	90	0.293	71.8
120	0.121	88.3	120	0.185	76.9
150	0.096	90.7	150	0.178	82.9
180	0.095	90.7	180	0.176	83.0
210	0.095	90.7	210	0.176	83.0

Appendix Table 8. % Degradation of MB dye under visible irradiation using ZnO-Ag_3PO_4-Fe_2O_3 (80:10:10) photocatalyst at different initial dye concentration. Catalyst load= 0.14 g, at pH= 6.

10 mg/L			**15 mg/L**			**20 mg/L**			**25 mg/L**		
Time(min)	Abs.	%	Time(min)	Abs.	%	Time(min)	Abs.	%	Time(min)	Abs.	%
0	1.041	0	0	1.498	0	0	1.978	0	0	2.508	0
30	0.688	34.6	30	1.243	17	30	1.604	18.9	30	2.017	19.5
60	0.362	65.5	60	1.088	27.3	60	1.335	32.5	60	1.336	46.7
90	0.141	86.5	90	0.57	61.9	90	1.078	45.5	90	0.976	61
120	0.121	88.4	120	0.352	76.5	120	0.734	62.8	120	0.77	69.2
150	0.096	90.8	150	0.205	86.3	150	0.348	82.4	150	0.529	78.9
180	0.095	90.8	180	0.205	86.3	180	0.346	82.5	180	0.528	78.9
210	0.095	90.8	210	0.205	86.3	210	0.346	82.5	210	0.528	78.9

Appendix Table 9. Percentage degradation of real sample sewage from Haile Garment Textile Industry swage tanker under visible irradiation using ZnO-Ag_3PO_4-Fe_2O_3 (80:10:10) photocatalyst.

Time(min)	**Abs**	**%**
0	1.041	0
30	0.856	17.7
60	0.74	28.9
90	0.619	40.5
120	0.321	69.1
150	0.291	72
180	0.290	72.1
210	0.290	72.1

Appendix Table 10. UV-Vis spectra result of 20 mg/L MB dye at different irradiation time

Wave length (nm)	Absorbance Before irradiation	Absorbance at 30 min irradiation	Absorbance At 60 min irradiation	Absorbance at 90 min irradiation	Absorbance at 120 min irradiation	Absorbance at 150 min irradiation
200	0.27	0.17	0.07	0.05	0.03	0.01
209	0.29	0.19	0.09	0.07	0.05	0.03
212	0.27	0.17	0.07	0.05	0.03	0.01
216	0.13	0.09	0.06	0.04	0.02	0.01
221	0.13	0.09	0.06	0.04	0.02	0.01
225	0.24	0.14	0.09	0.06	0.03	0.01
230	0.24	0.14	0.09	0.06	0.03	0.01
237	0.28	0.18	0.08	0.06	0.04	0.02
242	0.29	0.19	0.09	0.07	0.05	0.03
246	0.3	0.2	0.1	0.05	0.03	0.02
251	0.24	0.14	0.09	0.07	0.03	0.01
263	0.17	0.07	0.05	0.03	0.02	0.01
274	0.35	0.25	0.15	0.05	0.03	0.01
279	0.47	0.27	0.07	0.07	0.04	0.03
293	0.91	0.71	0.51	0.31	0.11	0.01
302	0.51	0.31	0.11	0.08	0.05	0.01
307	0.26	0.01	0.01	0.01	0.01	0.01
316	0.14	0.01	0.01	0.01	0.01	0.01
325	0.11	0.01	0.01	0.01	0.01	0.01
337	0.03	0.01	0.01	0.01	0.01	0.01
344	0.07	0.01	0.01	0.01	0.01	0.01
353	0.05	0.01	0.01	0.01	0.01	0.01
356	0.04	0.01	0.01	0.01	0.01	0.01
416	0.02	0.01	0.01	0.01	0.01	0.01
421	0.02	0.01	0.01	0.01	0.01	0.01
446	0.03	0.01	0.01	0.01	0.01	0.01
456	0.04	0.01	0.01	0.01	0.01	0.01
465	0.05	0.01	0.01	0.01	0.01	0.01
479	0.06	0.01	0.01	0.01	0.01	0.01
488	0.07	0.01	0.01	0.01	0.01	0.01
498	0.04	0.01	0.01	0.01	0.01	0.01
512	0.03	0.01	0.01	0.01	0.01	0.01
525	0.02	0.01	0.01	0.01	0.01	0.01
532	0.02	0.01	0.01	0.01	0.01	0.01
544	0.05	0.01	0.01	0.01	0.01	0.01
574	0.26	0.01	0.01	0.01	0.01	0.01
593	0.62	0.246	0.01	0.01	0.01	0.01
605	0.92	0.546	0.277	0.02	0.01	0.01
612	1.0	0.626	0.357	0.1	0.01	0.01
621	1.01	0.636	0.367	0.11	0.01	0.01

630	1.02	0.646	0.377	0.12	0.01	0.01
632	1.04	0.666	0.397	0.14	0.02	0.01
639	1.19	0.816	0.547	0.29	0.01	0.01
649	1.52	1.146	0.877	0.62	0.276	0.01
656	1.7	1.326	1.057	0.8	0.356	0.127
663	1.85	1.476	1.207	0.95	0.506	0.302
665	1.92	1.546	1.277	1.02	0.576	0.346
672	1.67	1.296	1.027	0.77	0.326	0.04
674	1.52	1.146	0.877	0.62	0.276	0.01
677	1.25	0.876	0.607	0.35	0.06	0.01
679	1.09	0.716	0.447	0.19	0.01	0.01
684	0.09	0.01	0.01	0.01	0.01	0.01
688	0.04	0.01	0.01	0.01	0.01	0.01
693	0.04	0.01	0.01	0.01	0.01	0.01
702	0.04	0.01	0.01	0.01	0.01	0.01
714	0.04	0.01	0.01	0.01	0.01	0.01
719	0.04	0.01	0.01	0.01	0.01	0.01
721	0.04	0.01	0.01	0.01	0.01	0.01
725	0.02	0.01	0.01	0.01	0.01	0.01
735	0.03	0.01	0.01	0.01	0.01	0.01
744	0.03	0.01	0.01	0.01	0.01	0.01
751	0.02	0.01	0.01	0.01	0.01	0.01
756	0.02	0.01	0.01	0.01	0.01	0.01
763	0.02	0.01	0.01	0.01	0.01	0.01
779	0.02	0.01	0.01	0.01	0.01	0.01
791	0.02	0.01	0.01	0.01	0.01	0.01
800	0.02	0.01	0.01	0.01	0.01	0.01

Figure 14. Preparation of ZnO-Ag_3PO_4-Fe_2O_3 ternary nanocomposite at different molar compositrion

Figure 15. Degradation of MB dye using ZnO-Ag_3PO_4-Fe_2O_3 (80:10:10) nano photo-catalyst.